

# UC Irvine

## UC Irvine Electronic Theses and Dissertations

### Title

Performance Comparison of Three Channel Charting Algorithms with Three Dimensionality Reduction Techniques in Quadriga Channels

### Permalink

<https://escholarship.org/uc/item/2q05m1rs>

### Author

Zhu, Wenyu

### Publication Date

2022

Peer reviewed|Thesis/dissertation

UNIVERSITY OF CALIFORNIA,  
IRVINE

Performance Comparison of Three Channel Charting Algorithms with Three  
Dimensionality Reduction Techniques in Quadriga Channels

THESIS

submitted in partial satisfaction of the requirements  
for the degree of

MASTER OF SCIENCE  
in Electrical Engineering

by

Wenyu Zhu

Thesis Committee:  
Professor Ender Ayanoglu, Chair  
Professor Filippo Capolino  
Professor Keyue Smedley

2022



# DEDICATION

To my mother



# TABLE OF CONTENTS

	Page
<b>LIST OF FIGURES</b>	<b>v</b>
<b>LIST OF TABLES</b>	<b>ix</b>
<b>ACKNOWLEDGMENTS</b>	<b>x</b>
<b>ABSTRACT OF THE THESIS</b>	<b>xi</b>
<b>1 Introduction</b>	<b>1</b>
1.1 Channel Charting . . . . .	1
<b>2 Pre-Processing Methods</b>	<b>2</b>
2.1 Method I: CSI Feature Extraction Method . . . . .	2
2.2 Method II: Efficient Distance Measure Method . . . . .	3
2.3 Method III: Correlation Matrix Distance Method . . . . .	5
<b>3 Dimensionality Reduction Methods</b>	<b>7</b>
3.1 Principal Component Analysis Method . . . . .	7
3.2 Sammon's Mapping Method . . . . .	8
3.3 Isomap Method . . . . .	9
<b>4 Experiments</b>	<b>10</b>
4.1 Performance Measures . . . . .	10
4.1.1 Continuity (CT) . . . . .	11
4.1.2 Trustworthiness (TW) . . . . .	12
4.1.3 Kruskal's Stress (KS) . . . . .	13
4.2 Simulation Setup . . . . .	14
4.2.1 Simulation I: 2D Scenario with 32 Antennas, 1 Subcarrier, 2.0GHz Center Carrier Frequency and 10MHz Bandwidth . . . . .	14
4.2.2 Simulation II: 3D Scenario with 32 Antennas, 1 Subcarrier, 2.0GHz Center Carrier Frequency and 10MHz Bandwidth . . . . .	15
4.2.3 Simulation III: 2D Scenario with 32 Antennas, 4 Subcarriers, 2.0GHz Center Carrier Frequency and 10MHz Bandwidth . . . . .	15

<b>5</b>	<b>Results</b>	<b>17</b>
5.1	Results of Simulation I . . . . .	18
5.1.1	Channel Chart under Q-LoS channels . . . . .	22
5.1.2	Performance Measures under Q-LoS channels . . . . .	25
5.1.3	Channel Chart under Q-NLoS channels . . . . .	28
5.1.4	Performance Measures under Q-NLoS channels . . . . .	31
5.2	Results of Simulation II . . . . .	34
5.2.1	Channel Chart under Q-LoS channels . . . . .	38
5.2.2	Performance Measures under Q-LoS channels . . . . .	41
5.2.3	Channel Chart under Q-NLoS channels . . . . .	44
5.2.4	Performance Measures under Q-NLoS channels . . . . .	47
5.3	Results of Simulation III . . . . .	50
5.3.1	Channel Chart under Q-LoS . . . . .	54
5.3.2	Performance Measures under Q-LoS channels . . . . .	57
5.3.3	Channel Chart under Q-NLoS channels . . . . .	60
5.3.4	Performance Measures under Q-NLoS channels . . . . .	63
<b>6</b>	<b>Conclusion</b>	<b>67</b>
	<b>Bibliography</b>	<b>68</b>

# LIST OF FIGURES

	Page
5.1 The user equipments' location in the real space in Simulation I. The colored points represent the user equipments, and the cross point represents the ULA.	20
5.2 The channel chart from Method I with PCA method under Q-LoS channels.	22
5.3 The channel chart from Method I with SM method under Q-LoS channels.	22
5.4 The channel chart from Method I with Isomap method under Q-LoS channels.	22
5.5 The channel chart from Method II with PCA method under Q-LoS channels.	23
5.6 The channel chart from Method II with SM method under Q-LoS channels.	23
5.7 The channel chart from Method II with Isomap method under Q-LoS channels.	23
5.8 The channel chart from Method III with PCA method under Q-LoS channels.	24
5.9 The channel chart from Method III with SM method under Q-LoS channels.	24
5.10 The channel chart from Method III with Isomap method under Q-LoS channels.	24
5.11 The continuity results from Method I with PCA, SM, and Isomap methods under Q-LoS channels.	25
5.12 The trustworthiness results from Method I with PCA, SM, and Isomap methods under Q-LoS channels.	25
5.13 The continuity results from Method II with PCA, SM, and Isomap methods under Q-LoS channels.	26
5.14 The trustworthiness results from Method II with PCA, SM, and Isomap methods under Q-LoS channels.	26
5.15 The continuity results from Method III with PCA, SM, and Isomap methods under Q-LoS channels.	27
5.16 The trustworthiness results from Method III with PCA, SM, and Isomap methods under Q-LoS channels.	27
5.17 The channel chart from Method I with PCA method under Q-NLoS channels.	28
5.18 The channel chart from Method I with SM method under Q-NLoS channels.	28
5.19 The channel chart from Method I with Isomap method under Q-NLoS channels.	28
5.20 The channel chart from Method II with PCA method under Q-NLoS channels.	29
5.21 The channel chart from Method II with SM method under Q-NLoS channels.	29
5.22 The channel chart from Method II with Isomap method under Q-NLoS channels.	29
5.23 The channel chart from Method III with PCA method under Q-NLoS channels.	30
5.24 The channel chart from Method III with SM method under Q-NLoS channels.	30
5.25 The channel chart from Method III with Isomap method under Q-NLoS channels.	30

5.26	The continuity results from Method I with PCA, SM, and Isomap methods under Q-NLoS channels. . . . .	31
5.27	The trustworthiness results from Method I with PCA, SM, and Isomap methods under Q-NLoS channels. . . . .	31
5.28	The continuity results from Method II with PCA, SM, and Isomap methods under Q-NLoS channels. . . . .	32
5.29	The trustworthiness results from Method II with PCA, SM, and Isomap methods under Q-NLoS channels. . . . .	32
5.30	The continuity results from Method III with PCA, SM, and Isomap methods under Q-NLoS channels. . . . .	33
5.31	The trustworthiness results from Method III with PCA, SM, and Isomap methods under Q-NLoS channels. . . . .	33
5.32	The user equipments' location in the real space in Simulation II. The colored points represent the user equipments, and the cross point represents the ULA.	36
5.33	The channel chart from Method I with PCA method under Q-LoS channels.	38
5.34	The channel chart from Method I with SM method under Q-LoS channels. .	38
5.35	The channel chart from Method I with Isomap method under Q-LoS channels.	38
5.36	The channel chart from Method II with PCA method under Q-LoS channels.	39
5.37	The channel chart from Method II with SM method under Q-LoS channels. .	39
5.38	The channel chart from Method II with Isomap method under Q-LoS channels.	39
5.39	The channel chart from Method III with PCA method under Q-LoS channels.	40
5.40	The channel chart from Method III with SM method under Q-LoS channels.	40
5.41	The channel chart from Method III with Isomap method under Q-LoS channels.	40
5.42	The continuity results from Method I with PCA, SM, and Isomap methods under Q-LoS channels. . . . .	41
5.43	The trustworthiness results from Method I with PCA, SM, and Isomap methods under Q-LoS channels. . . . .	41
5.44	The continuity results from Method II with PCA, SM, and Isomap methods under Q-LoS channels. . . . .	42
5.45	The trustworthiness results from Method II with PCA, SM, and Isomap methods under Q-LoS channels. . . . .	42
5.46	The continuity results from Method III with PCA, SM, and Isomap methods under Q-LoS channels. . . . .	43
5.47	The trustworthiness results from Method III with PCA, SM, and Isomap methods under Q-LoS channels. . . . .	43
5.48	The channel chart from Method I with PCA method under Q-NLoS channels.	44
5.49	The channel chart from Method I with SM method under Q-NLoS channels.	44
5.50	The channel chart from Method I with Isomap method under Q-NLoS channels.	44
5.51	The channel chart from Method II with PCA method under Q-NLoS channels.	45
5.52	The channel chart from Method II with SM method under Q-NLoS channels.	45
5.53	The channel chart from Method II with Isomap method under Q-NLoS channels.	45
5.54	The channel chart from Method III with PCA method under Q-NLoS channels.	46
5.55	The channel chart from Method III with SM method under Q-NLoS channels.	46
5.56	The channel chart from Method III with Isomap method under Q-NLoS channels. . . . .	46

5.57	The continuity results from Method I with PCA, SM, and Isomap methods under Q-NLoS channels. . . . .	47
5.58	The trustworthiness results from Method I with PCA, SM, and Isomap methods under Q-NLoS channels. . . . .	47
5.59	The continuity results from Method II with PCA, SM, and Isomap methods under Q-NLoS channels. . . . .	48
5.60	The trustworthiness results from Method II with PCA, SM, and Isomap methods under Q-NLoS channels. . . . .	48
5.61	The continuity results from Method III with PCA, SM, and Isomap methods under Q-NLoS channels. . . . .	49
5.62	The trustworthiness results from Method III with PCA, SM, and Isomap methods under Q-NLoS channels. . . . .	49
5.63	The user equipments' location in the real space in Simulation III. The colored points represent the user equipments, and the cross point represents the ULA.	52
5.64	The channel chart from Method I with PCA method under Q-LoS channels.	54
5.65	The channel chart from Method I with SM method under Q-LoS channels. .	54
5.66	The channel chart from Method I with Isomap method under Q-LoS channels.	54
5.67	The channel chart from Method II with PCA method under Q-LoS channels.	55
5.68	The channel chart from Method II with SM method under Q-LoS channels. .	55
5.69	The channel chart from Method II with Isomap method under Q-LoS channels.	55
5.70	The channel chart from Method III with PCA method under Q-LoS channels.	56
5.71	The channel chart from Method III with SM method under Q-LoS channels.	56
5.72	The channel chart from Method III with Isomap method under Q-LoS channels.	56
5.73	The continuity results from Method I with PCA, SM, and Isomap methods under Q-LoS channels. . . . .	57
5.74	The trustworthiness results from Method I with PCA, SM, and Isomap methods under Q-LoS channels. . . . .	57
5.75	The continuity results from Method II with PCA, SM, and Isomap methods under Q-LoS channels. . . . .	58
5.76	The trustworthiness results from Method II with PCA, SM, and Isomap methods under Q-LoS channels. . . . .	58
5.77	The continuity results from Method III with PCA, SM, and Isomap methods under Q-LoS channels. . . . .	59
5.78	The trustworthiness results from Method III with PCA, SM, and Isomap methods under Q-LoS channels. . . . .	59
5.79	The channel chart from Method I with PCA method under Q-NLoS channels.	60
5.80	The channel chart from Method I with SM method under Q-NLoS channels.	60
5.81	The channel chart from Method I with Isomap method under Q-NLoS channels.	60
5.82	The channel chart from Method II with PCA method under Q-NLoS channels.	61
5.83	The channel chart from Method II with SM method under Q-NLoS channels.	61
5.84	The channel chart from Method II with Isomap method under Q-NLoS channels.	61
5.85	The channel chart from Method III with PCA method under Q-NLoS channels.	62
5.86	The channel chart from Method III with SM method under Q-NLoS channels.	62
5.87	The channel chart from Method III with Isomap method under Q-NLoS channels. . . . .	62

5.88	The continuity results from Method I with PCA, SM, and Isomap methods under Q-NLoS channels. . . . .	63
5.89	The trustworthiness results from Method I with PCA, SM, and Isomap methods under Q-NLoS channels. . . . .	63
5.90	The continuity results from Method II with PCA, SM, and Isomap methods under Q-NLoS channels. . . . .	64
5.91	The trustworthiness results from Method II with PCA, SM, and Isomap methods under Q-NLoS channels. . . . .	64
5.92	The continuity results from Method III with PCA, SM, and Isomap methods under Q-NLoS channels. . . . .	65
5.93	The trustworthiness results from Method III with PCA, SM, and Isomap methods under Q-NLoS channels. . . . .	65

# LIST OF TABLES

	Page
4.1 The scenario and parameters setting used in Simulation I. . . . .	15
4.2 The scenario and parameters setting used in Simulation II. . . . .	16
4.3 The scenario and parameters setting used in Simulation III. . . . .	16
5.1 The performances of KS under the Q-LoS channels and the Q-NLoS channels. Method I represents the CSI extracted features method proposed in [7]. Method II represents the distance measurement method proposed in [5]. Method III represents the correlation matrix distance method. . . . .	21
5.2 The performances of KS under the Q-LoS channels and the Q-NLoS channels. Method I represents the CSI extracted features method proposed in [7]. Method II represents the distance measurement method proposed in [5]. Method III represents the correlation matrix distance method. . . . .	36
5.3 The performances of KS under the Q-LoS channels and the Q-NLoS channels. Method I represents the CSI extracted features method proposed in [7]. Method II represents the distance measurement method proposed in [5]. Method III represents the correlation matrix distance method. . . . .	53

# ACKNOWLEDGMENTS

First of all, I would like to extend my deep thanks to my supervisor Professor Ender Ayanoglu, who has offered me numerous valuable suggestions with incomparable patience and encouraged me profoundly throughout my graduate study.

Secondly, I also want to express my thanks to Amr Aly, who worked in the some other aspects of this topic in cooperation with me which are not shown in this thesis.

Finally, I am deeply indebted to my mother and close friends, whose encouragement and support have made my accomplishments possible.



# ABSTRACT OF THE THESIS

Performance Comparison of Three Channel Charting Algorithms with Three Dimensionality Reduction Techniques in Quadriga Channels

By

Wenyu Zhu

MASTER OF SCIENCE in Electrical Engineering

University of California, Irvine, 2022

Professor Ender Ayanoglu, Chair

Channel charting, is a novel unsupervised machine learning method to get the representation of multiple transmit locations to reflect the local “radio geometry” by processing the channel state information with a dimensionality reduction method. In this thesis, channel charting results in three different channel charting algorithms, channel state information (CSI) feature extraction method, efficient distance measure method, and correlation matrix distance (CMD) method, together with three dimensionality reduction methods, principal component analysis (PCA), sammon’s Mapping (SM), and Isomap, under two Quadriga channel models, line-of-sight (Q-LoS) model and a non-line-of-sight (Q-NLoS) model, are presented. In order to evaluate the quality of the performance of these nine alternative methods, three performance measures, continuity, trustworthiness. and Kruskal’s stress, are considered. The simulations are set under both 2-dimension and 3-dimension scenario, and also under single subcarrier and multi-subcarriers. Several observations are made from these simulation results.

# Chapter 1

## Introduction

### 1.1 Channel Charting

With the development of the new generation of wireless communication systems, future wireless communication systems should be able to provide ultra-reliable and low-latency services with massive throughput.

Currently, machine learning is widely used in solving wireless communication problems, like location finding. However, these techniques work successfully with some location information known before, as kind of learning materials. Channel charting is an emerging framework, first proposed in [7], as an unsupervised technology to describe the radio geometry of a specific area, only based on the slowly time varying channel state information (CSI) transmitted from the user equipments (UEs) inside. Unlike those commonly used machine learning techniques, the most significant feature of channel charting is its non-supervisory nature. Channel charting could learn the relative locations of the transmitters, like how close between two user equipments, without knowing the exact location information of a little cluster of transmitters.

# Chapter 2

## Pre-Processing Methods

The main idea of channel charting is to extract low dimensional radio geometry from the received high dimensional channel state information, the channel chart, representing user equipment locations and their neighborhood relationships. However, due to path loss in transmission, we cannot directly use the acquired CSI to compute the true distances between UEs. We need to do some pre-processing operations to eliminate these effects. Here we introduce three pre-processing methods.

### 2.1 Method I: CSI Feature Extraction Method

CSI feature extraction method, proposed in [7], includes two steps, feature extraction and feature transform. We denote  $\mathbf{h} \in \mathbb{C}^M$  as the received CSI vector transmitted from user equipments, and  $\mathbf{h}_i \in \mathbb{C}^M$  is the CSI vector received at the time sample  $i$ ; matrix  $\mathbf{H}$  is the collection of  $\mathbf{h}$ , collected from  $N$  user equipments. We compute the raw second moment (R2M) of the CSI matrix,  $\bar{\mathbf{H}} = \mathbb{E}[\mathbf{h}\mathbf{h}^H]$ , to eliminate the influence of noise, interference, and potential variations. To be more practical, we average the received CSI vectors over a

period of short time. Therefore, the raw second moment becomes  $\bar{\mathbf{H}} = \frac{1}{T} \sum_{t=1}^T \mathbf{h}_t \mathbf{h}_t^H$ , where  $T$  is the number of sample stamps. The scaled raw second moment matrix  $\tilde{\mathbf{H}}$  is defined as following:

$$\tilde{\mathbf{H}} = \frac{A^{\beta-1}}{\|\bar{\mathbf{H}}\|_F^\beta} \bar{\mathbf{H}} \quad (2.1)$$

where  $\beta = 1 + 1/(2\sigma)$  and  $\|\cdot\|_F$  represents the Frobenius distance. After scaling the R2M matrix, the distance between two user equipments,  $A$  and  $B$ , calculated from the scaled R2M matrix could reflect the real spatial geometry. We will have

$$d_h(\tilde{\mathbf{H}}_A, \tilde{\mathbf{H}}_B) = \|\tilde{\mathbf{H}}_A - \tilde{\mathbf{H}}_B\|_F, \quad (2.2)$$

here we could consider,

$$d_h(\tilde{\mathbf{H}}_A, \tilde{\mathbf{H}}_B) = |d_A - d_B|. \quad (2.3)$$

In order to improve the performance of the channel chart, applying discrete Fourier transform (DFT) to the scaled R2M matrix  $\tilde{\mathbf{H}}$ , transforming the CSI features from the antenna domain to the angular domain to get the channel feature matrix  $\mathbf{F}$ .

## 2.2 Method II: Efficient Distance Measure Method

In reference [5], the author proposed a new pre-processing method, which could solve the problem that the distance computing from the received CSI directly could not reveal the true locations of the user equipments. The author gives a new distance measurement, defined

below

$$d_h(\mathbf{h}_A, \mathbf{h}_B)^* \triangleq \min_{\phi \in [0, 2\pi]} \left\| \frac{\mathbf{h}_A}{\|\mathbf{h}_A\|_2} - e^{j\phi} \frac{\mathbf{h}_B}{\|\mathbf{h}_B\|_2} \right\|_2^2 \quad (2.4)$$

where  $\|\cdot\|_2$  represents the Euclidean distance. Here,  $d_h(\mathbf{h}_A, \mathbf{h}_B)^*$  changes with the distance between user equipment A and B monotonically, so it can be used to represent the distance between two user equipments. However, it is not an easy task to find the minimum value between these normalized CSI vectors. Considering the fact that the real part of a complex number is always no greater than its magnitude, we could get

$$\begin{aligned} & \left\| \frac{\mathbf{h}_A}{\|\mathbf{h}_A\|_2} - e^{j\phi} \frac{\mathbf{h}_B}{\|\mathbf{h}_B\|_2} \right\|_2^2 \\ &= \frac{\|\mathbf{h}_A\|_2 \|\mathbf{h}_B\|_2 - e^{j\phi} \mathbf{h}_B^H \mathbf{h}_A\|_2^2}{\|\mathbf{h}_A\|_2^2 \|\mathbf{h}_B\|_2^2} \\ &= \frac{(\mathbf{h}_A \|\mathbf{h}_B\|_2 - e^{j\phi} \mathbf{h}_B \|\mathbf{h}_A\|_2) (\mathbf{h}_A^H \|\mathbf{h}_B\|_2 - e^{-j\phi} \mathbf{h}_B^H \|\mathbf{h}_A\|_2)}{\|\mathbf{h}_A\|_2^2 \|\mathbf{h}_B\|_2^2} \\ &= \frac{\mathbf{h}_A \mathbf{h}_A^H \|\mathbf{h}_B\|_2^2 + \mathbf{h}_B \mathbf{h}_B^H \|\mathbf{h}_A\|_2^2 - (e^{j\phi} \mathbf{h}_A^H \mathbf{h}_B \|\mathbf{h}_A\|_2 \|\mathbf{h}_B\|_2 + e^{-j\phi} \mathbf{h}_A \mathbf{h}_B^H \|\mathbf{h}_A\|_2 \|\mathbf{h}_B\|_2)}{\|\mathbf{h}_A\|_2^2 \|\mathbf{h}_B\|_2^2} \\ &= 2 - \frac{e^{j\phi} \mathbf{h}_A^H \mathbf{h}_B + e^{-j\phi} \mathbf{h}_A \mathbf{h}_B^H}{\|\mathbf{h}_A\|_2 \|\mathbf{h}_B\|_2} \\ &\leq 2 - 2 \frac{|\mathbf{h}_A^H \mathbf{h}_B|}{\|\mathbf{h}_A\|_2 \|\mathbf{h}_B\|_2}. \end{aligned}$$

So we could get the simplified distance measurement formula shown in the reference [5]

$$d_h(\mathbf{h}_A, \mathbf{h}_B)^* = 2 - 2 \frac{|\mathbf{h}_A^H \mathbf{h}_B|}{\|\mathbf{h}_A\|_2 \|\mathbf{h}_B\|_2}. \quad (2.5)$$

This method is insensitive to small scale fading and keeps part of sensitivity to absolute direction and delay with a low dimension, which greatly simplifies the computation.

## 2.3 Method III: Correlation Matrix Distance Method

In [3], the authors introduce another distance measure, correlation matrix distance (CMD), for MIMO channels, for analyzing the change in the structure of the channels. First, considering a zero-mean stochastic signal vector  $\mathbf{h}(t)$ , the correlation matrix of this signal vector is

$$\mathbf{R}(\mathbf{t}) = E \{ \mathbf{x}(t) \mathbf{x}(t)^H \}. \quad (2.6)$$

Moreover, as the inner product of two matrices equals the trace of the product of these matrices, considering the inner product between two correlation matrices from two different time stamps, we will get an inequality relationship

$$\langle \mathbf{R}(t_1) \mathbf{R}(t_2) \rangle = \text{tr} \{ \mathbf{R}(t_1) \mathbf{R}(t_2) \}, \quad (2.7)$$

$$\langle \mathbf{R}(t_1) \mathbf{R}(t_2) \rangle \leq \| \mathbf{R}(t_1) \|_2 \| \mathbf{R}(t_2) \|_2. \quad (2.8)$$

Therefore, we could get

$$0 \leq \frac{\text{tr} \{ \mathbf{R}(t_1) \mathbf{R}(t_2) \}}{\| \mathbf{R}(t_1) \|_2 \| \mathbf{R}(t_2) \|_2} \leq 1. \quad (2.9)$$

Based on the above inequality relationship, the author gives the definition of the correlation matrix distance:

$$d_{corr}(t_1, t_2) = 1 - \frac{\text{tr} \{ \mathbf{R}(t_1) \mathbf{R}(t_2) \}}{\| \mathbf{R}(t_1) \|_2 \| \mathbf{R}(t_2) \|_2}. \quad (2.10)$$

The correlation matrix distance could also be used for calculating the full channel correlation matrix, and the definition of the full channel correlation matrix is

$$\mathbf{R}_H = E \left\{ \text{vec} \{ \mathbf{H} \} \text{vec} \{ \mathbf{H} \}^H \right\}. \quad (2.11)$$

From (2.10) and (2.11) above, we get

$$d_{cmd}(\mathbf{H}_A, \mathbf{H}_B) = 1 - \frac{\text{tr}(\mathbf{H}_A^H \mathbf{H}_B)}{\|\mathbf{H}_A\|_2 \|\mathbf{H}_B\|_2}. \quad (2.12)$$

From the inequality (2.9) above, it is apparent that the correlation matrix distance ranges from 0 to 1, and the more orthogonal  $\mathbf{H}_A$  and  $\mathbf{H}_B$  are, the correlation matrix distance is more close to 1.

# Chapter 3

## Dimensionality Reduction Methods

In Chapter 2, we introduce three pre-processing methods to process the CSI vectors received from the ULA array to eliminate some noise in the path and correct the relative location between user equipments due to the path loss and small signal fading. Furthermore, in this chapter, we will introduce three dimensionality reduction methods to process the CSI vectors in the second part, converting the high dimension CSI vectors to low dimension, and visual location coordinates in the channel chart.

### 3.1 Principal Component Analysis Method

Principal component analysis (PCA) is the most commonly used linear dimensionality reduction method. Its goal is to map high-dimensional data into a low-dimensional space through some linear projection aiming for the most information about the data in the projected dimension, thus using lower data dimensions while retaining more of the original data features. Consider we have  $M$  samples  $\{\mathbf{X}^1, \mathbf{X}^2, \dots, \mathbf{X}^M\}$ , and each sample  $\mathbf{X}^i$  has  $N$  features  $\mathbf{X}^i = (x_1^i, x_2^i, \dots, x_N^i)^T$ . First, we calculate the mean of each row, and then subtract the



corresponding mean value to center each feature, so that we could get a new feature matrix  $\bar{\mathbf{X}}$ . And then we calculate the covariance matrix of  $\bar{\mathbf{X}}$ . And we compute the eigenvalues and the eigenvectors of this covariance matrix, order the eigenvalues in a diagonal matrix in descending order, and follow this order to concatenate the corresponding eigenvectors as the new base matrix. Finally, we project the original samples  $\{\mathbf{X}^1, \mathbf{X}^2, \dots, \mathbf{X}^M\}$  onto this new base matrix to get the low dimension representing matrix  $\mathbf{Z} = [\mathbf{z}_1, \mathbf{z}_2, \dots, \mathbf{z}_N]$ , here  $N$  is our desired reduced dimension.

## 3.2 Sammon's Mapping Method

Sammon's mapping (SM), unlike PCA, is a classical nonlinear dimensionality reduction method, which could preserve the structure of the high dimension data points when reflecting on the low dimension points. We denote the distance between the  $i$ th and  $j$ th data point in the original space as  $d_{ij}^*$ , and the distance between the  $i$ th and  $j$ th data point in the low dimension space as  $d_{ij}$ . We then define the error function

$$E = \frac{1}{\sum_{i < j} d_{ij}^*} \sum_{i < j} \frac{(d_{ij}^* - d_{ij})^2}{d_{ij}^*}. \quad (3.1)$$

The goal of the SM method is to minimize this error function. Compared with the PCA method, the SM method cares more about preserving the pairwise distance when reflecting the high dimension data points to low dimension data points. So, obviously, SM could preserve more structure of the data distance and relationships between data points with the trade-off of increasing the computation complexity.

### 3.3 Isomap Method

Both the PCA and the SM methods are classical dimensionality reduction methods widely used in the Euclidean space. However, Isomap [8] provides a nonlinear dimensionality reduction way to process the data embedding in a manifold surface. The main idea of the Isomap is similar to another classical dimensionality reduction method, multidimensional scaling (MDS), but it uses another way of distance measure to fit the data embedded in a manifold surface. Intuitively, when considering the distance between two data points, we will use the Euclidean distance. However, when we consider the distance between two data points in the Isomap method, the Euclidean distance does not work perfectly, as the Euclidean distance might show a distance in the space, but not on the manifold surface, which is the true distance between the two data points. Hence, we try to use a set of polylines with a distance that is small enough so that the Euclidean distance is close to the true distance linking two other points in the manifold surface to represent the distance between two points in the manifold surface. So here, for each data point, we assume that the  $K$  smallest Euclidean distances between the point itself and other data points are the true distances, and set the distance between other point pairs to zero, and then based on these  $K$  distances to build the adjacent matrix  $G$ . We then applied the Dijkstra algorithm to compute the shortest distances between all pairs of user points to get a final shortest paths distances matrix  $D_G$ . For each pairwise distance added into the adjacent matrix  $G$ , it is always the minimum distance it could reach. We substitute the shortest paths distances matrix  $D_G$  for the distance matrix  $D$  in the multidimensional scaling method, performing feature decomposition on the intermediate matrix  $B$  computing from  $G$  to get the low dimension representing results. In the simulation, we use the function `sklearn.manifold.Isomap` [6] to process the input distance matrix to generate the channel chart.

# Chapter 4

## Experiments

In Chapter 2, we introduced three CSI pre-processing methods, and in Chapter 3, we introduced three dimensionality reduction methods. In this chapter, we will set experiments to evaluate the quality of the channel charts generated from the different combinations among pre-processing methods and dimensionality reduction methods. We will introduce three channel chart performance measures, and the setting of the scenario with parameters used in the experiments.

### 4.1 Performance Measures

For the techniques to be evaluated in this thesis, we are not going to evaluate the absolute positions of the channel chart, but rather the local performance of the generated channel chart, which means we focus more on whether the generated channel chart preserves the original neighborhood relationships rather than whether the locations of the user equipments in the generated channel chart are close to their true positions in reality. From this perspective, a certain degree of translation or rotation is acceptable.

We denote the location coordinates vector of the user equipments in the real space as  $\{\mathbf{u}_n\}_{n=1}^N$ , and denote the coordinates vector from the channel chart as  $\{\mathbf{v}_n\}_{n=1}^N$ . Here,  $\mathbf{u}_i$  and  $\mathbf{v}_i$  have one-to-one correspondence. For a point  $\mathbf{u}_i$  in the real space, its representation in the channel chart is  $\mathbf{v}_i$ . As we want to consider the local performance of a single point, for a specific point  $\mathbf{u}_i$  or  $\mathbf{v}_i$ , we consider the relationship between the point itself and its  $K$ -nearest neighbors. Considering a point  $\mathbf{u}_i$  in the original space, we denote the collection of the  $K$ th nearest neighbors of  $\mathbf{u}_i$  as  $\mathcal{V}_K(\mathbf{u}_i)$ , so that the points in the set  $\mathcal{V}_K(\mathbf{u}_i)$  have the  $K$ th shortest distance among all the observed user equipments (points). And now we focus on the rank of these distances between the points in the set  $\mathcal{V}_K(\mathbf{u}_i)$  and  $\mathbf{u}_i$ . We denote this rank of distance between a point  $\mathbf{u}_j$  in the set  $\mathcal{V}_K(\mathbf{u}_i)$  and  $\mathbf{u}_i$  as  $r(i, j)$ . We assume the rank of the distance between  $\mathbf{u}_j$  and  $\mathbf{u}_i$  is  $p$ , which means among all the distances between other points and the point  $\mathbf{u}_i$ , the distance between  $\mathbf{u}_j$  and  $\mathbf{u}_i$  is the  $p$ th shortest distance. Hence, we could assign the value of the rank  $r(i, j) = p$ . In the channel chart, we have similar definitions in the real space. For a point  $\mathbf{v}_i$  in the channel chart, we define the set of its  $K$ th nearest neighbors as  $\mathcal{U}_K(\mathbf{v}_i)$  and the rank of the distance between a point  $\mathbf{v}_j$  in the set  $\mathcal{U}_K(\mathbf{v}_i)$  and the point  $\mathbf{v}_i$  is denoted as  $\hat{r}(i, j)$ .

#### 4.1.1 Continuity (CT)

Continuity (CT) aims to measure how well the channel chart is in keeping the local neighborhood relationships in real space. Therefore, we consider a point  $\mathbf{u}_i$  in the real space and all its  $K$ -neighbors in the set  $\mathcal{V}_K(\mathbf{u}_i)$ , and we know that the distance rank  $r(i, j)$  of the points in the set  $\mathcal{V}_K(\mathbf{u}_i)$  is from 1 to  $k$ , so we want to find out the distance rank  $\hat{r}(i, j)$  in the channel chart between the representation point of  $\mathbf{u}_i$ ,  $\mathbf{v}_i$ , and the representation point of the points

in the set  $\mathcal{V}_K(\mathbf{u}_i)$ . So here we give the definition of continuity of a point  $\mathbf{u}_i$

$$\mathbf{CT}_i(K) = 1 - \frac{2}{K(2N - 3K - 1)} \sum_{j \in \mathcal{V}_K(\mathbf{u}_i)} (\hat{r}(i, j) - K). \quad (4.1)$$

From the definition of continuity of a single point  $\mathbf{u}_i$ , by averaging the continuity of each observed points in the target area, we can easily get the definition of the global continuity

$$\mathbf{CT}(K) = \frac{1}{N} \sum_{i=1}^N \mathbf{CT}_i(K). \quad (4.2)$$

Both the single point continuity and the global continuity range from 0 to 1, and if  $\mathbf{CT}(K)$  is close to 0, we can say that the performance of the generated channel chart is not good in continuity, and if  $\mathbf{CT}(K)$  is close to 1, the performance of the generated channel chart is good in continuity.

#### 4.1.2 Trustworthiness (TW)

Trustworthiness (TW) is to measure whether the channel chart creates non-existent neighborhood relationships in real space. Hence we consider a point  $\mathbf{v}_i$  in the channel chart and all its  $K$ -neighbors in the set  $\mathcal{U}_K(\mathbf{v}_i)$ , and we consider the most  $k$  top distance rank  $\hat{r}(i, j)$  of the points in the set  $\mathcal{U}_K(\mathbf{v}_i)$  in the channel chart, so that we find the corresponding distance rank  $r(i, j)$  in the real space and put them into the definition formula of the trustworthiness

$$\mathbf{TW}_i(K) = 1 - \frac{2}{K(2N - 3K - 1)} \sum_{j \in \mathcal{U}_K(\mathbf{v}_i)} (r(i, j) - K). \quad (4.3)$$

The above definition is the trustworthiness of the single point  $\mathbf{v}_i$ . Similarly, we average the trustworthiness value from all the point in the channel chart, and we could get the global

trustworthiness

$$\mathbf{TW}(K) = \frac{1}{N} \sum_{i=1}^N \mathbf{TW}_i(K). \quad (4.4)$$

Both the single point trustworthiness and the global trustworthiness are in the range of zero to one. If the value of the trustworthiness is low, representing that the channel chart creates more non-existent neighborhood relationships in the real space. If the value of the trustworthiness is high, representing that the channel chart creates less non-existent neighborhood relationship in the real space. So that we will know that when the trustworthiness is close to one, the channel chart has better performance while when the trustworthiness is close to zero, the channel chart has worse performance.

### 4.1.3 Kruskal's Stress (KS)

Kruskal's stress (KS), first proposed in [4], is to measure how well the distance in the channel chart representing the distance in the real space is, globally. Unlike the measure of the continuity and trustworthiness, Kruskal's stress considers all the point pairs in the observing area, but not limited neighborhood pairs. Here we give the definition of the Kruskal's stress [2]

$$\mathbf{KS} = \sqrt{\frac{\sum_{i,j} (\|\mathbf{u}_j - \mathbf{u}_i\| - \beta \|\mathbf{v}_j - \mathbf{v}_i\|)^2}{\sum_{i,j} \|\mathbf{u}_j - \mathbf{u}_i\|^2}}, \quad (4.5)$$

$$\beta = \frac{\sum_{i,j} \|\mathbf{u}_j - \mathbf{u}_i\| \|\mathbf{v}_j - \mathbf{v}_i\|}{\sum_{i,j} \|\mathbf{v}_j - \mathbf{v}_i\|^2}.$$

The Kruskal's stress also ranges between zero and one. However, unlike the performance measure in continuity and trustworthiness, if Kruskal's stress is more close to zero, it means

the performance of the channel chart is better while if Kruskal's stress is more close to one, it means the performance of the channel chart is worse.

## 4.2 Simulation Setup

In this section, we will introduce the simulation setup, including the simulation scenario and the simulation parameters. The main parameters are provided in [7, Table I]. For each simulation setting, we simulated all nine method combinations (three pre-processing method *times* three dimensionality reduction methods) under two kinds of Quadriga channel models[1], the Q-LoS channel model and the Q-NLoS channel model.

### 4.2.1 Simulation I: 2D Scenario with 32 Antennas, 1 Subcarrier, 2.0GHz Center Carrier Frequency and 10MHz Bandwidth

In Simulation I, we first consider a 2D scenario, the number of user equipments  $N = 2048$  where UEs are randomly located in a  $1000\text{m} \times 500\text{m}$  plane, and a uniform linear array (ULA) with  $A = 32$  antennas and  $S = 1$  subcarrier ( $M = AS$ ) to acquire CSI at SNR = 0 dB averaging over 10 samples. The ULA is at the origin of the plane of the UEs, 100m away from the square area where the UEs are located. The center carrier frequency is  $f_c = 2.0\text{GHz}$  with a bandwidth of  $BW = 10\text{MHz}$ . All the parameters we used are shown in Table 4.1 below:

Parameter	Setting
Scenario	2D BERLIN_UMa_LOS & BERLIN_UMa_NLOS
Number of UEs	$N = 2048$
Number of antennas	$A = 32$
Number of subcarriers	$S = 1$
Carrier frequency	$f_c = 2.0\text{GHz}$
Bandwidth	$BW = 10\text{MHz}$
Antenna array	ULA with $\Delta r = \lambda/2$
Number of neighbors	$K = 30$
SNR	SNR = 0 dB
Number of samples	10

Table 4.1: The scenario and parameters setting used in Simulation I.

#### 4.2.2 Simulation II: 3D Scenario with 32 Antennas, 1 Subcarrier, 2.0GHz Center Carrier Frequency and 10MHz Bandwidth

In Simulation II, we use the same parameter setting as that is in Simulation I. We have  $A = 32$  antennas,  $S = 1$  subcarrier,  $f_c = 2.0\text{GHz}$  center carrier frequency and  $BW = 10\text{MHz}$  bandwidth. However, in this 3D scenario, we want to exam how the space location affects the results by changing the relative position between the ULA and the user equipments. We move the ULA up to 10 meters from the horizontal plane, co-located with the user equipments to 10 meters above the plane where the user equipments located. As the angle between the ULA array and the user equipments changes, the receiving CSI information will change consequently, so that the channel chart results might be changed. All the parameters we used are shown in Table 4.2 below:

#### 4.2.3 Simulation III: 2D Scenario with 32 Antennas, 4 Subcarriers, 2.0GHz Center Carrier Frequency and 10MHz Bandwidth

In Simulation III, we use another set of parameters. We want to test how these alternatives perform in multi-subcarriers case. So, the parameters change to  $A = 32$  antennas,  $S = 4$



Parameter	Setting
Scenario	3D BERLIN_UMa_LOS & BERLIN_UMa_NLOS
Number of UEs	$N = 2048$
Number of antennas	$A = 32$
Number of subcarriers	$S = 1$
Carrier frequency	$f_c = 2.0\text{GHz}$
Bandwidth	$BW = 10\text{MHz}$
Antenna array	ULA with $\Delta r = \lambda/2$
Number of neighbors	$K = 30$
SNR	SNR = 0 dB
Number of samples	10

Table 4.2: The scenario and parameters setting used in Simulation II.

subcarriers,  $f_c = 2.0\text{GHz}$  center carrier frequency and  $BW = 10\text{MHz}$  bandwidth. We simulate in the 2D scenario, setting the ULA located on the same horizontal plane with the user equipments. All the parameters we used are shown in Table 4.3 below:

Parameter	Setting
Scenario	2D BERLIN_UMa_LOS & BERLIN_UMa_NLOS
Number of UEs	$N = 2048$
Number of antennas	$A = 32$
Number of subcarriers	$S = 4$
Carrier frequency	$f_c = 2.0\text{GHz}$
Bandwidth	$BW = 10\text{MHz}$
Antenna array	ULA with $\Delta r = \lambda/2$
Number of neighbors	$K = 30$
SNR	SNR = 0 dB
Number of samples	10

Table 4.3: The scenario and parameters setting used in Simulation III.

# Chapter 5

## Results

In Chapter 4, we define three channel chart measures, continuity (CT), trustworthiness (TW), and Kruskal's stress (KS), to evaluate the results generated from different methods combinations, and we give the simulation settings. In this chapter, we will show the results from the simulation we introduce in Chapter 4 and compare the performances among different techniques. For each simulation results, we first present 9 channel charts from 9 alternative methods, and the user equipment's point in the real space figure with its corresponding representation point in the channel chart has the same color. And then we present the continuity and the trustworthiness performance comparison figures among the PCA, SM, and Isomap methods for all three pre-processing methods. In these figures, the blue line represents the results of the PCA method, the red line represents the results of the SM method, and the green line represents the results of the Isomap method.

## 5.1 Results of Simulation I

First, we consider the results under the Q-LoS channels. Fig. 5.2 - Fig. 5.4 are the channel charts with Method I of PCA method, SM method, and Isomap method. The channel chart from the SM method visually shows better preservation of the spacial geometry than the channel chart from the PCA and Isomap methods. And from Fig. 5.11 and Fig. 5.12, we observe consistency. The red line, the CT or TW results from the SM method, is higher than the blue line and the green line, the CT or TW results from the PCA and Isomap method, respectively. Fig. 5.5 - Fig. 5.7 are the channel charts with Method II of PCA method, SM method, and Isomap method. Compared with the corresponding channel charts with Method I, Fig. 5.2 - Fig. 5.4, the channel charts with Method II look no better than those with Method I. The points in the channel chart from Method II are more dispersed. First we consider the CT results with Method II. Fig. 5.13 shows that the SM results are still better than those results from the PCA method and the Isomap method. Comparing Fig. 5.13 with Fig. 5.11, the CT results with Method II from the PCA method and the SM method close, and when the number of nearest neighbors is small, are better than the corresponding results with Method I. The CT results with Method II from the Isomap method are much better than those results with Method I. And then we consider the TW results with Method II. Fig. 5.14 shows that the results from the Isomap method are always the worst, but when the number of nearest neighbors is small,  $K \leq 64$ , approximately, the results from the SM method are the best, while when the number of nearest neighbors increases,  $K > 64$ , approximately, the results from the PCA method go higher, becoming the best. When comparing Fig. 5.14 with Fig. 5.12, we find that the corresponding lines in the Fig. 5.14 are much higher than those in the Fig. 5.12. This means the TW results with Method II are much better than those with Method I from every dimensionality reduction method. Fig. 5.8 - Fig. 5.10 are the channel charts with Method III of PCA method, SM method, and Isomap method. Generally, the channel charts with Method III look similar to those

with Method II. However, the channel chart from Method III with the PCA method seems to have a horizontal flip with the channel chart from Method II with the PCA method. In Fig. 5.9, the points in the channel chart from Method III with the SM method are much more scattered than the points in Fig. 5.6 from Method II. In Fig. 5.10, the points from the Isomap method are a little bit more concentrated than the points in Fig. 5.7. Therefore, we could observe in Fig. 5.15 and Fig. 5.16, the red lines and the blue lines are quite similar to the corresponding lines in Fig. 5.13 and Fig. 5.14. Whereas the green lines in Fig. 5.15 and Fig. 5.16, the results from the Isomap method, are much higher than the corresponding green lines in Fig. 5.13 and Fig. 5.14, which is consistent with what we observe from the channel charts.

Second, we consider the results under the Q-NLoS channels. Fig. 5.17 - Fig. 5.19 are the channel charts with Method I of PCA method, SM method, and Isomap method. The channel chart from the SM method still looks better than the channel chart from the PCA method and the Isomap method visually. And the channel chart from the PCA method looks close to the channel chart from the Isomap method. However, the CT and TW results give other observations. In Fig. 5.26 and Fig. 5.27, the green lines, results from the Isomap method, are above the blues lines and red lines in both two figures, which means the channel chart from the Isomap method keeps more neighborhood relationships information than the other two dimensionality reduction methods, although from the channel chart we cannot observe. However, these increases in both the CT and TW results are slight. Fig. 5.20 - Fig. 5.22 are the channel charts with Method II of PCA method, SM method, and Isomap method. The channel chart from Method II with the PCA method and the channel chart from Method I with the PCA method are flipped upside down. Compared to Fig. 5.18, the channel chart from Method II with the SM method rotated about  $90^\circ$  counterclockwise. Compared with Fig. 5.19, the channel chart from Method II with the Isomap method flips horizontally. In Fig. 5.28 and Fig. 5.29, the blue lines are on the top. And compared with Fig. 5.26, we find that both the CT and TW results from Method II with the PCA method and the SM method

are higher than those from Method I with the PCA method and the SM method, respectively, while the CT and TW results from Method II with the Isomap method are lower than those from Method I with the Isomap method. Fig. 5.23 - Fig. 5.25 are the channel charts with Method III of PCA method, SM method, and Isomap method. The channel chart, the CT results, and the TW results from Method III of all three dimensionality reduction methods are quite similar to those from Method II, respectively.

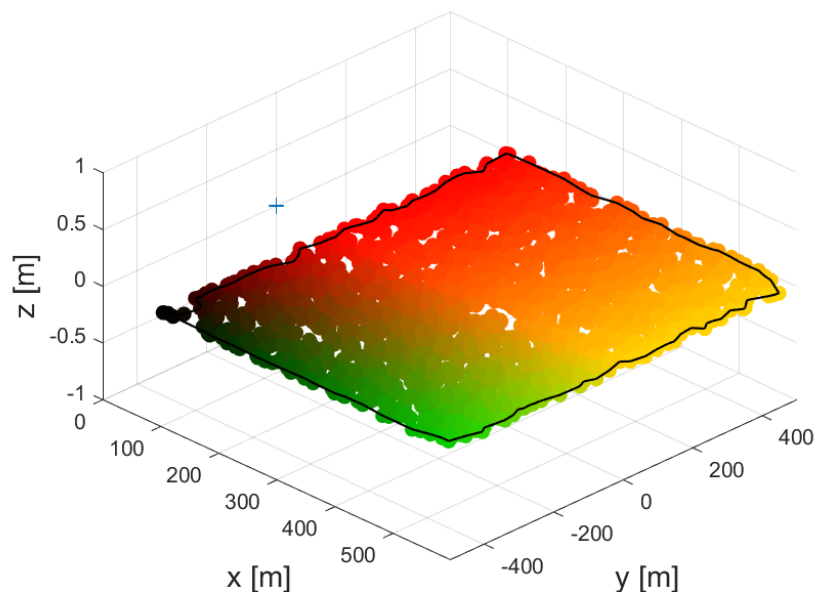


Figure 5.1: The user equipments' location in the real space in Simulation I. The colored points represent the user equipments, and the cross point represents the ULA.

Under the Q-LoS channels, the CT and TW results from the Isomap method always give the worst performance, while those results from PCA and SM are close. We could also find that the CT and TW results from Method II are close to those from Method III, but much better than those corresponding results from Method I. However, under the Q-NLoS channels, the case is slightly different. The CT and TW results with the PCA and SM methods from Method II are also close to those from Method III, better than those from Method I. However, for the Isomap method, in Method I, the CT and TW results are the best among all the three dimensionality reduction methods, but still lower than those results

from the PCA and SM method with Method II and Method III. The KS results have a different pattern other than those in CT and TW.

Under both Q-LoS and Q-NLoS channels, the differences among the KS results from the PCA method and the SM method with all three pre-processing methods are very slight. However, the KS results from the Isomap method are much lower than those others, especially with the Method III, which means, from the view of the KS, the Isomap method gives better performance in preserving the local pair-wise relationships existing in real space.

	Method	I	II	III
Q-LoS	PCA	0.4624	0.4848	0.4817
	SM	0.4775	0.4973	0.4930
	Isomap	0.4997	0.4535	0.4376
Q-NLoS	PCA	0.4654	0.4509	0.4530
	SM	0.4665	0.4649	0.4641
	Isomap	0.4622	0.4080	0.4018

Table 5.1: The performances of KS under the Q-LoS channels and the Q-NLoS channels. Method I represents the CSI extracted features method proposed in [7]. Method II represents the distance measurement method proposed in [5]. Method III represents the correlation matrix distance method.

### 5.1.1 Channel Chart under Q-LoS channels

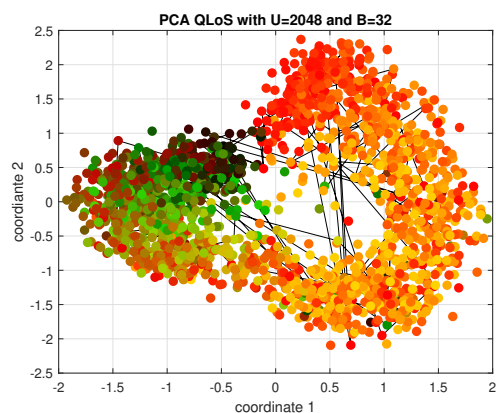


Figure 5.2: The channel chart from Method I with PCA method under Q-LoS channels.

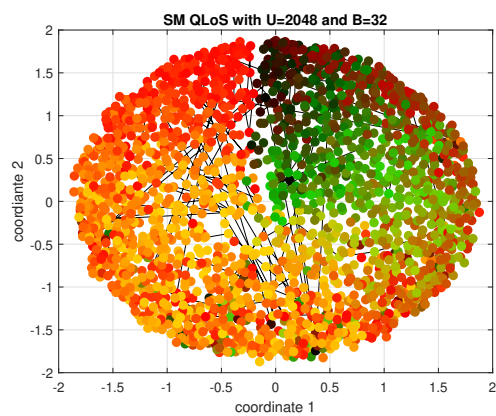


Figure 5.3: The channel chart from Method I with SM method under Q-LoS channels.

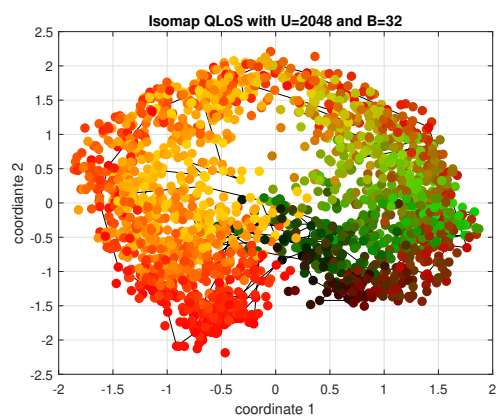


Figure 5.4: The channel chart from Method I with Isomap method under Q-LoS channels.

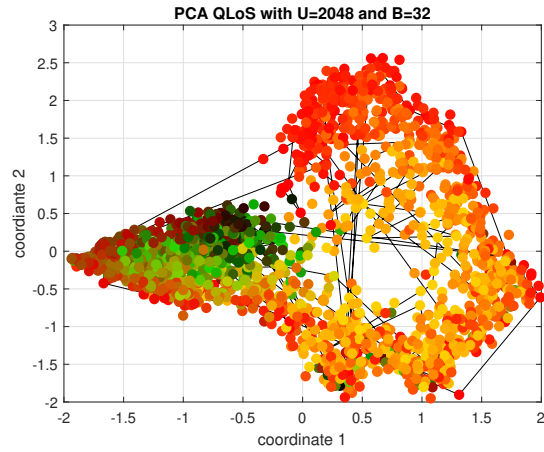


Figure 5.5: The channel chart from Method II with PCA method under Q-LoS channels.

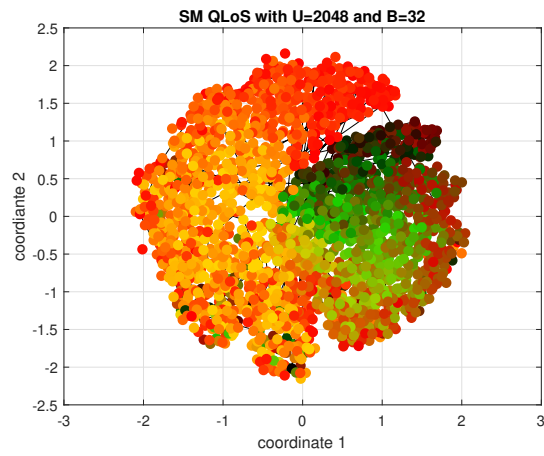


Figure 5.6: The channel chart from Method II with SM method under Q-LoS channels.

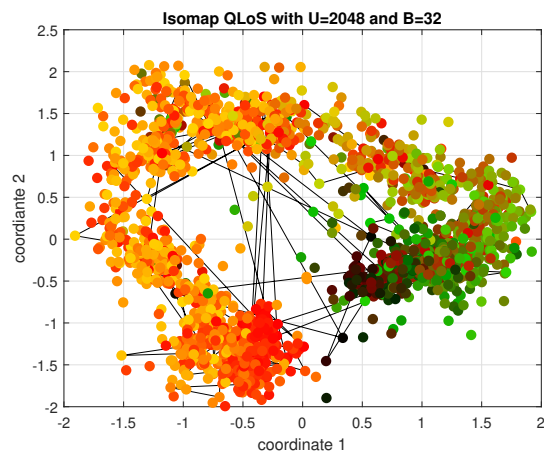


Figure 5.7: The channel chart from Method II with Isomap method under Q-LoS channels.



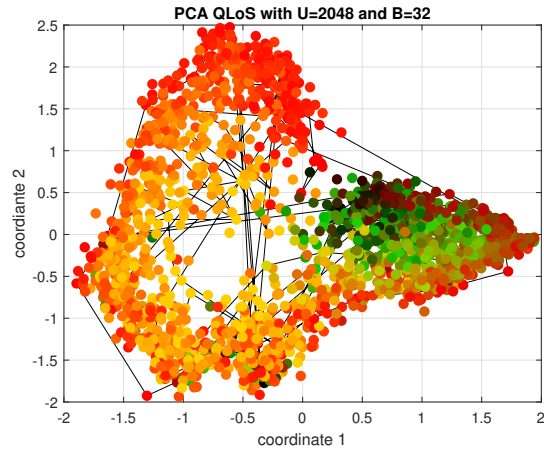


Figure 5.8: The channel chart from Method III with PCA method under Q-LoS channels.

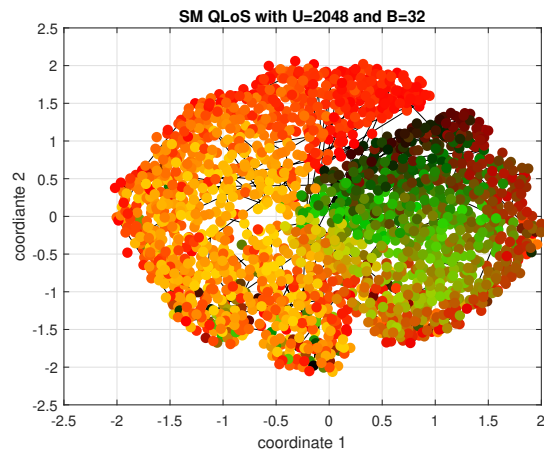


Figure 5.9: The channel chart from Method III with SM method under Q-LoS channels.

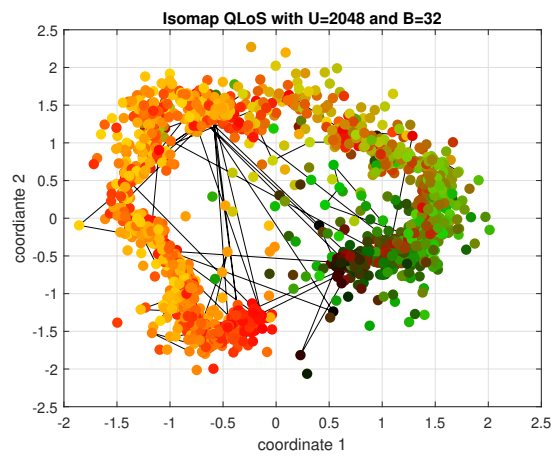


Figure 5.10: The channel chart from Method III with Isomap method under Q-LoS channels.

## 5.1.2 Performance Measures under Q-LoS channels

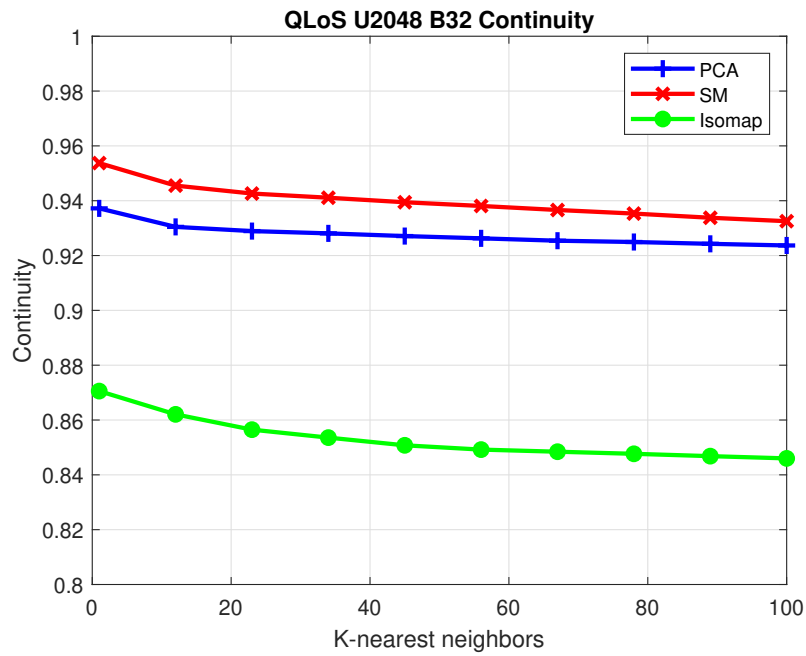


Figure 5.11: The continuity results from Method I with PCA, SM, and Isomap methods under Q-LoS channels.

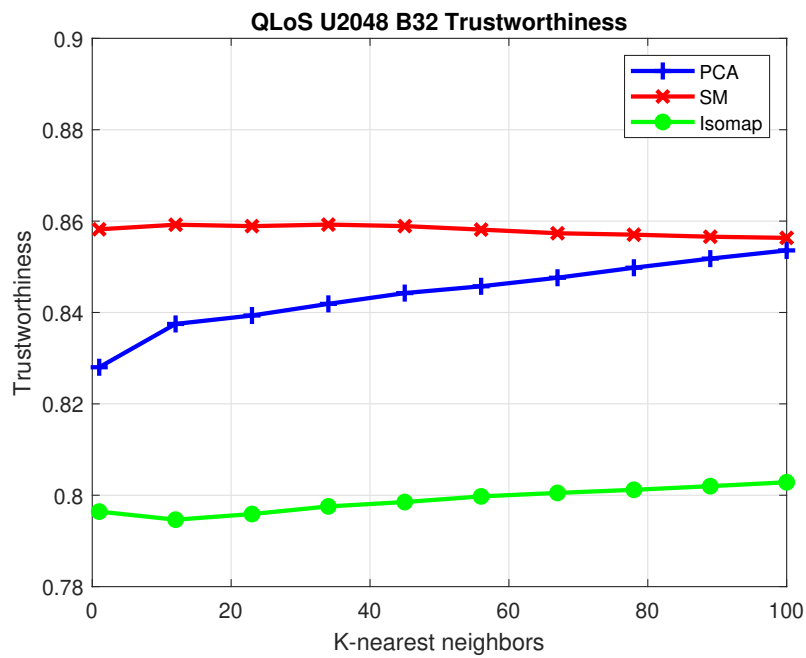


Figure 5.12: The trustworthiness results from Method I with PCA, SM, and Isomap methods under Q-LoS channels.

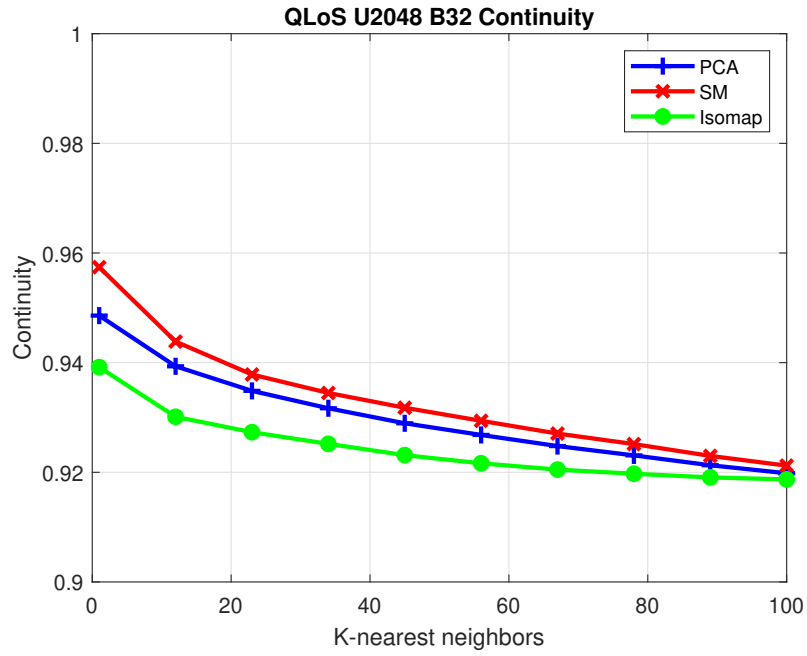


Figure 5.13: The continuity results from Method II with PCA, SM, and Isomap methods under Q-LoS channels.

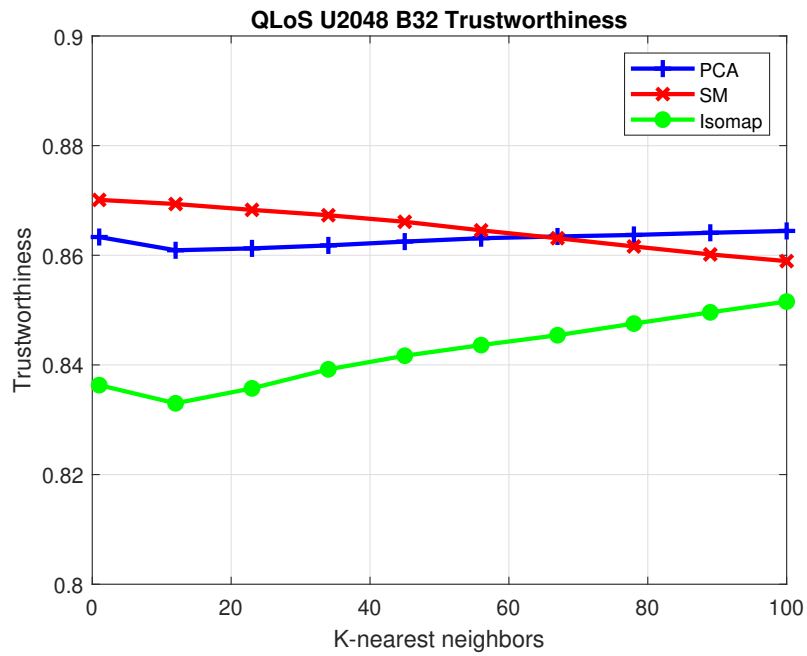


Figure 5.14: The trustworthiness results from Method II with PCA, SM, and Isomap methods under Q-LoS channels.

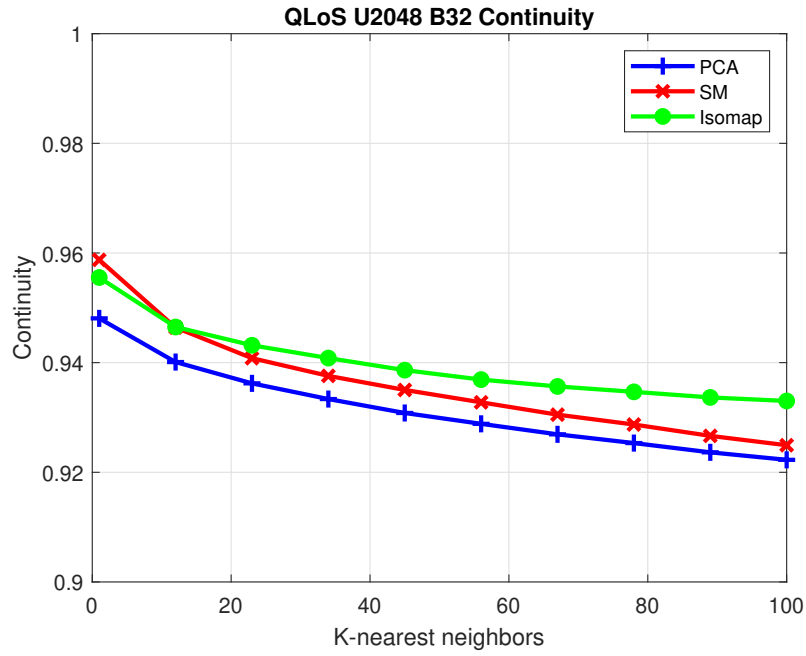


Figure 5.15: The continuity results from Method III with PCA, SM, and Isomap methods under Q-LoS channels.

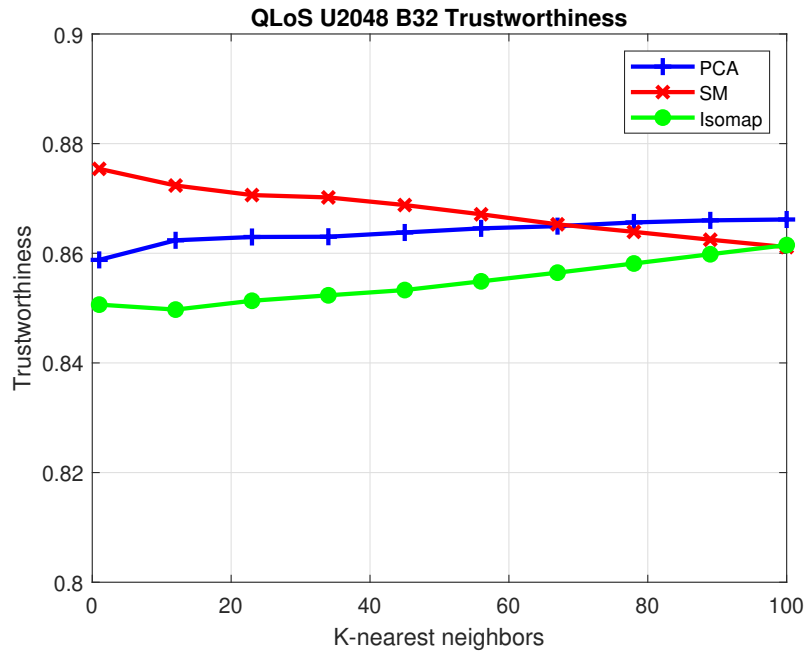


Figure 5.16: The trustworthiness results from Method III with PCA, SM, and Isomap methods under Q-LoS channels.

### 5.1.3 Channel Chart under Q-NLoS channels

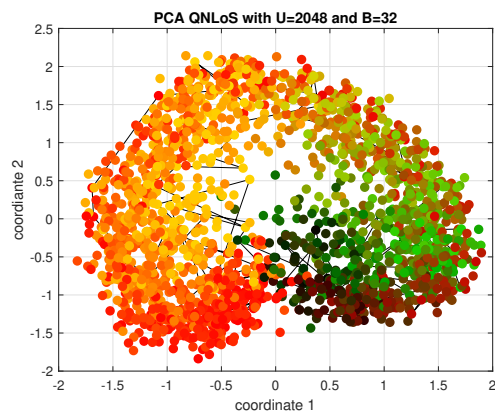


Figure 5.17: The channel chart from Method I with PCA method under Q-NLoS channels.

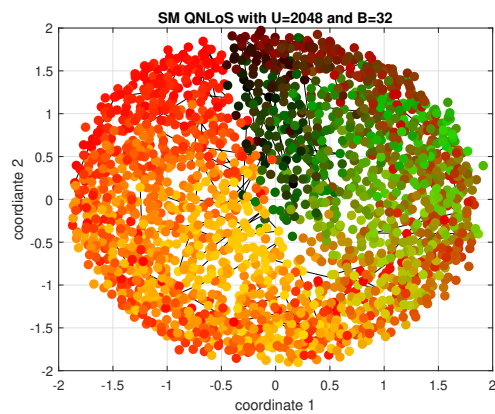


Figure 5.18: The channel chart from Method I with SM method under Q-NLoS channels.

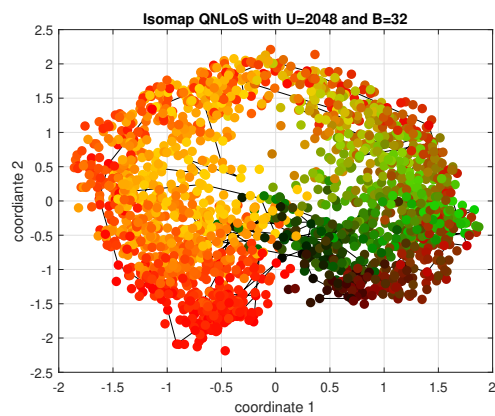


Figure 5.19: The channel chart from Method I with Isomap method under Q-NLoS channels.

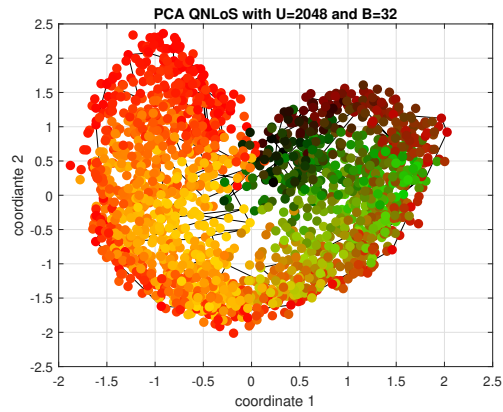


Figure 5.20: The channel chart from Method II with PCA method under Q-NLoS channels.

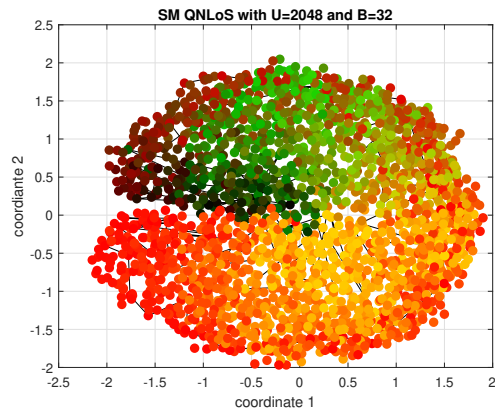


Figure 5.21: The channel chart from Method II with SM method under Q-NLoS channels.

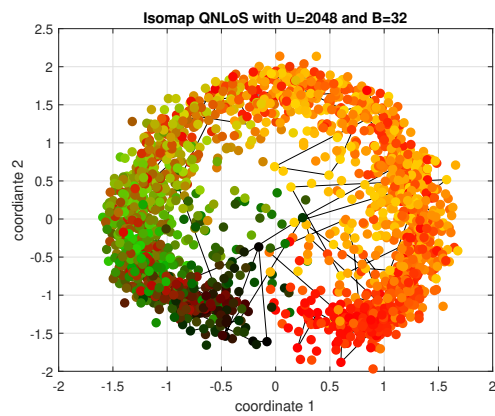


Figure 5.22: The channel chart from Method II with Isomap method under Q-NLoS channels.

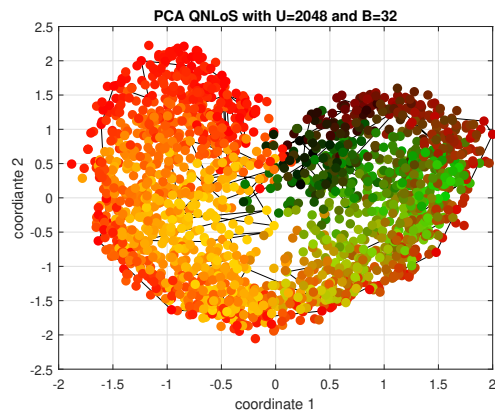


Figure 5.23: The channel chart from Method III with PCA method under Q-NLoS channels.

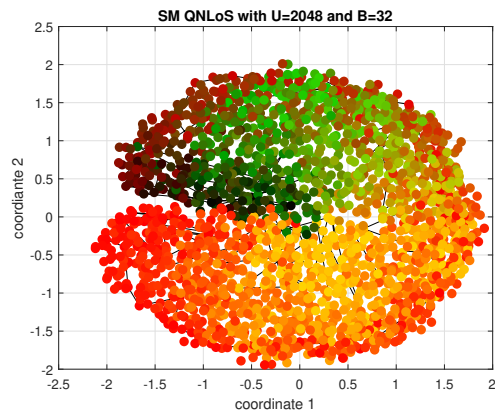


Figure 5.24: The channel chart from Method III with SM method under Q-NLoS channels.

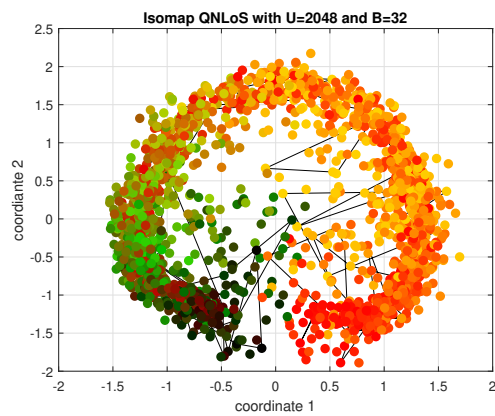


Figure 5.25: The channel chart from Method III with Isomap method under Q-NLoS channels.

### 5.1.4 Performance Measures under Q-NLoS channels

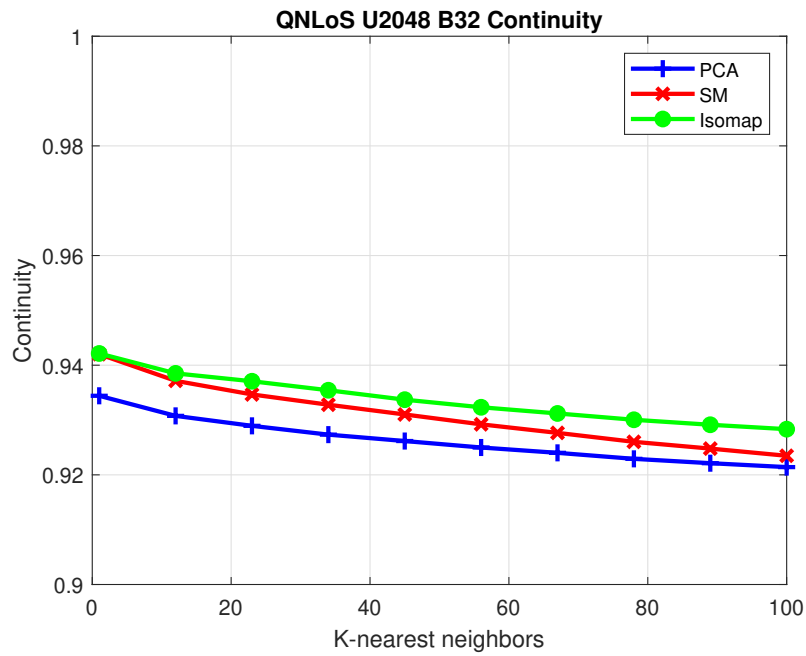


Figure 5.26: The continuity results from Method I with PCA, SM, and Isomap methods under Q-NLoS channels.

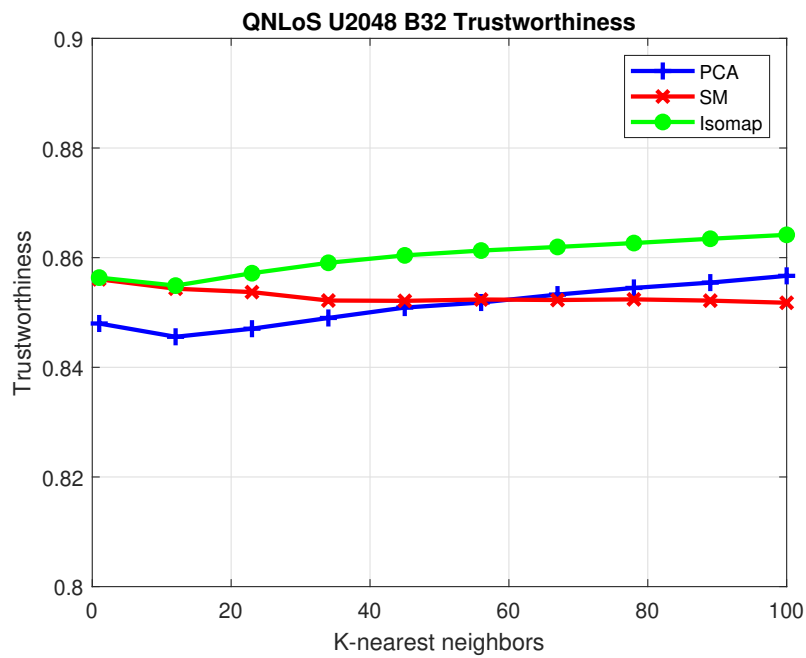


Figure 5.27: The trustworthiness results from Method I with PCA, SM, and Isomap methods under Q-NLoS channels.



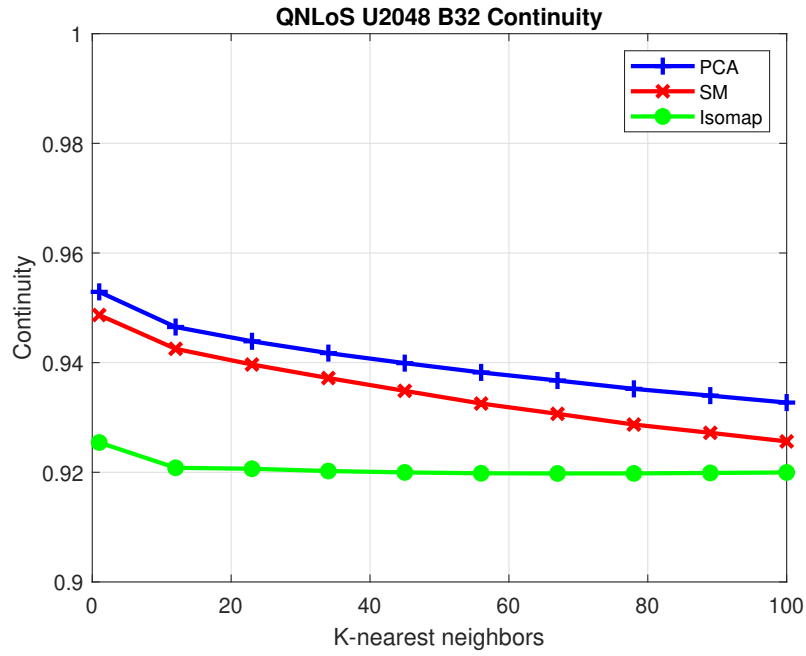


Figure 5.28: The continuity results from Method II with PCA, SM, and Isomap methods under Q-NLoS channels.

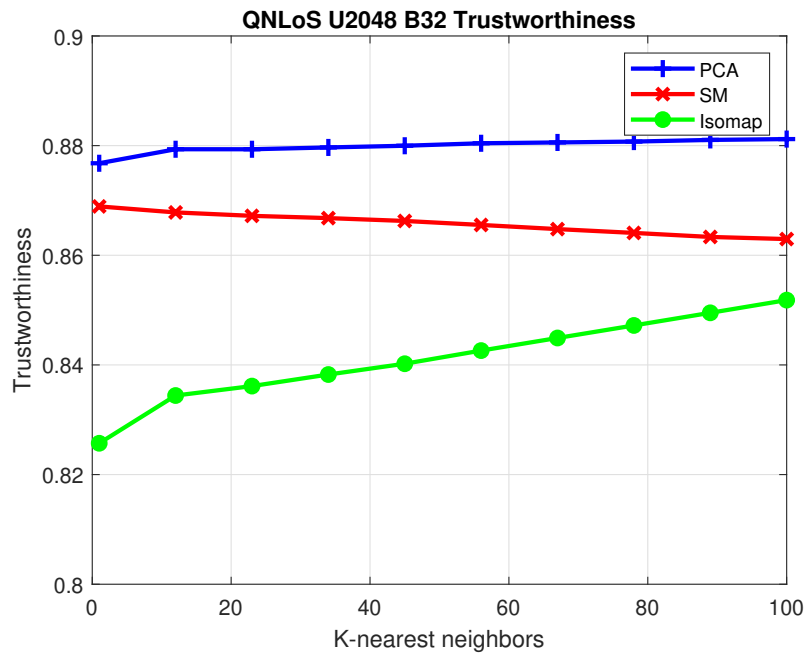


Figure 5.29: The trustworthiness results from Method II with PCA, SM, and Isomap methods under Q-NLoS channels.

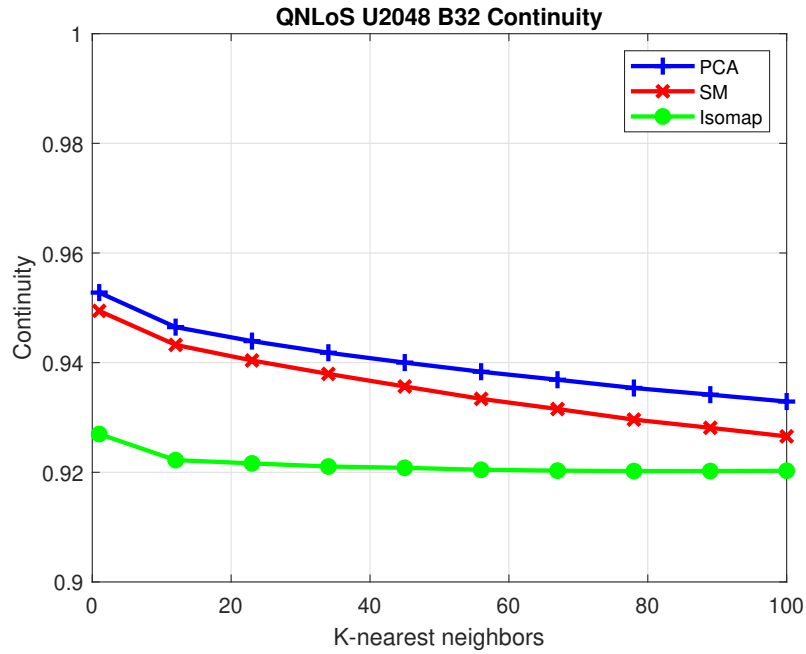


Figure 5.30: The continuity results from Method III with PCA, SM, and Isomap methods under Q-NLoS channels.

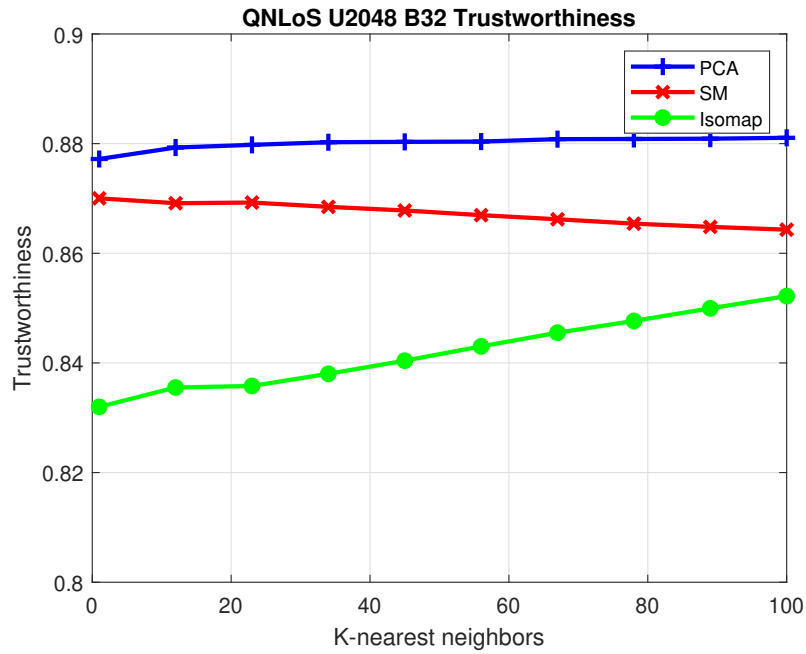


Figure 5.31: The trustworthiness results from Method III with PCA, SM, and Isomap methods under Q-NLoS channels.

## 5.2 Results of Simulation II

First, we consider the results under the Q-LoS channels. Fig. 5.33 - Fig. 5.35 are the channel charts with Method I of PCA method, SM method, and Isomap method. The channel chart from the SM method seems to be the best among these three channel charts. And compared with Fig. 5.35, the points in Fig. 5.35 are more messy. However, in Fig. 5.42, the CT results from the SM method and the Isomap method are close, and are better than the CT results from the PCA method. In Fig. 5.43, when the number of the nearest neighbors is small,  $K \leq 30$ , approximately, the TW results from the SM method and the Isomap results are close, while when the number of the nearest neighbors becomes larger,  $K > 30$ , approximately, the TW results from the Isomap method increase continuously, which are higher than those from the SM method. The TW results from the PCA method are still the worst. Fig. 5.36 - Fig. 5.38 are the channel charts with Method II of PCA method, SM method, and Isomap method. Compared with Fig. 5.33 - Fig. 5.35, the points in the channel chart from Method II are more disordered. However, when we consider the CT and TW results, the conditions are different. In Fig. 5.44, the CT results from Method II with the PCA method and the SM method are higher than those from Method I with the PCA method and the SM method. Whereas the results from Method II with the Isomap method are lower than those from Method I with the Isomap method. In Fig. 5.45, the TW results from Method II with the PCA method and the SM method are higher than those from Method I with the PCA method and the SM method. When the number of the nearest neighbors  $K \leq 67$ , the TW results from the SM method are the highest, while the number of the nearest neighbors  $K > 67$ , the TW results from the PCA method are the highest. The TW results from the Isomap method are the worst. Fig. 5.39 - Fig. 5.41 are the channel charts with Method III of PCA method, SM method, and Isomap method. From the channel chart view, the performance of Fig. 5.39 - Fig. 5.41 are worse than those of Fig. 5.33 - Fig. 5.35. In Fig. 5.46, the CT results from Method III with the PCA method

and the SM method are similar to those from Method II with the PCA method and the SM method. The CT results from Method III with the Isomap method are higher than those results from Method I and Method II with the Isomap method. In Fig. 5.47, the TW results from Method III with the PCA method and the SM method are close to those from Method II with the PCA method and the SM method. The TW results from Method III with the Isomap method are higher than those results from Method II but lower than those results from Method I with the Isomap method.

And second, we consider the results under the Q-NLoS channels. Fig. 5.48 - Fig. 5.50 are the channel charts with Method I of PCA method, SM method, and Isomap method. Similarly, the channel chart from the SM method looks better. In Fig. 5.57 and Fig. 5.58, the CT and TW results from the Isomap methods are the best among all three dimensionality reduction methods, while those results from the PCA method are the worst among all three dimensionality reduction methods. Fig. 5.51 - Fig. 5.53 are the channel charts with Method II of PCA method, SM method, and Isomap method. The channel charts from Method II look worse than those from Method I. However, in Fig. 5.59 and Fig. 5.60, the CT and TW results from Method II with the PCA method and the SM method are close, and higher than those from Method I with the PCA method and the SM method, respectively, while the CT and TW results from Method II with the Isomap method are the worst, and worse than those from Method II with Isomap method. Fig. 5.51 - Fig. 5.53 are the channel charts with Method III of PCA method, SM method, and Isomap method. Although the channel charts from Method III look quite different from those corresponding channel charts from Method II, the CT and TW results from Method III are similar to those corresponding results from Method II.

The results of Simulation II, the 3D scenario are quite similar to but no better than those of Simulation I, the 2D scenario. First, we consider the CT and TW results. We find that under Q-LoS channels, the results with Isomap using Method I provide better performance

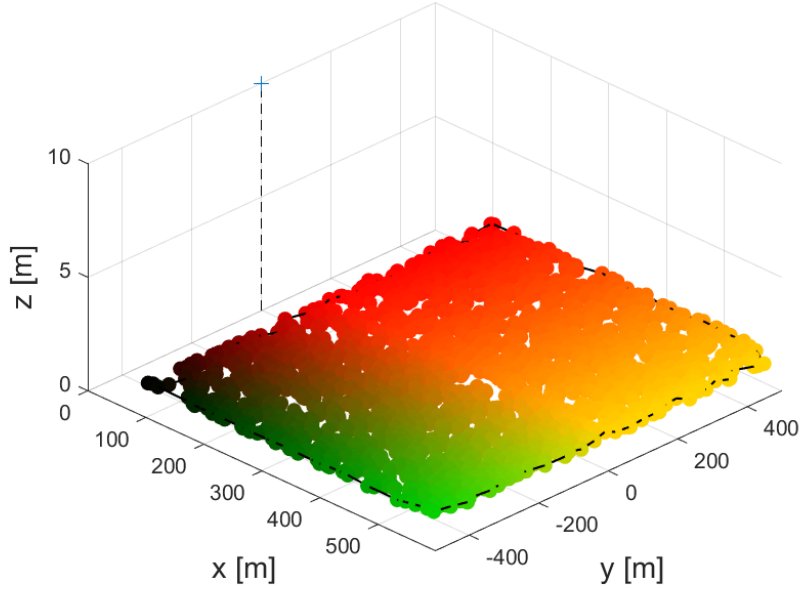


Figure 5.32: The user equipments' location in the real space in Simulation II. The colored points represent the user equipments, and the cross point represents the ULA.

	Method	I	II	III
Q-LoS	PCA	0.4624	0.4817	0.4817
	SM	0.4775	0.4931	0.4930
	Isomap	0.4944	0.4535	0.4376
Q-NLoS	PCA	0.4796	0.4837	0.4837
	SM	0.4846	0.4915	0.4915
	Isomap	0.4638	0.4358	0.4266

Table 5.2: The performances of KS under the Q-LoS channels and the Q-NLoS channels. Method I represents the CSI extracted features method proposed in [7]. Method II represents the distance measurement method proposed in [5]. Method III represents the correlation matrix distance method.

than these results with PCA and SM slightly while the results with PCA and SM using Method II or Method III, are slightly better than those corresponding results with Isomap. But the CT results with Isomap using Method III are better than those with PCA and SM when the number of neighbors increases. Under the Q-NLoS channels, the gap is wider. The CT and TW results with Isomap using Method I are much better than those with PCA and SM while the results with PCA and SM using Method II or Method III are much better than these with Isomap. However, the KS results do not have much difference comparing with these from Simulation I and follow the same rules like what we discuss in the Simulation I's conclusions. The KS results with all other alternatives are close, while the KS results with Isomap using Method II and Method III show a significant improvement.

## 5.2.1 Channel Chart under Q-LoS channels

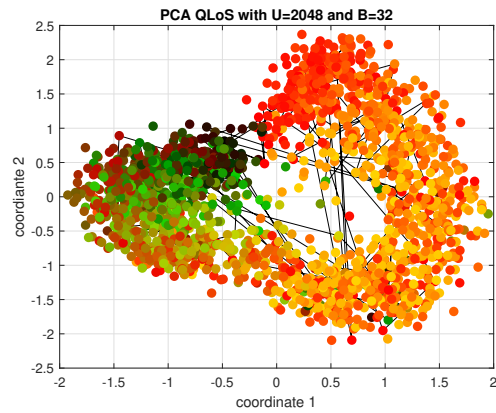


Figure 5.33: The channel chart from Method I with PCA method under Q-LoS channels.

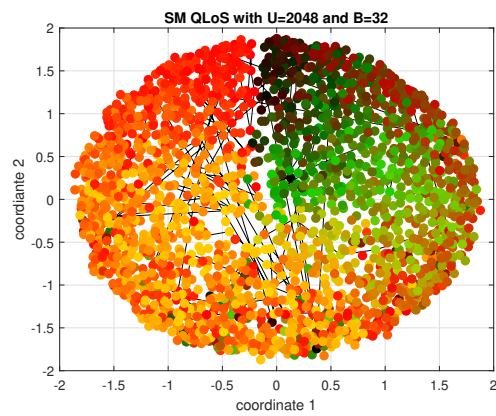


Figure 5.34: The channel chart from Method I with SM method under Q-LoS channels.

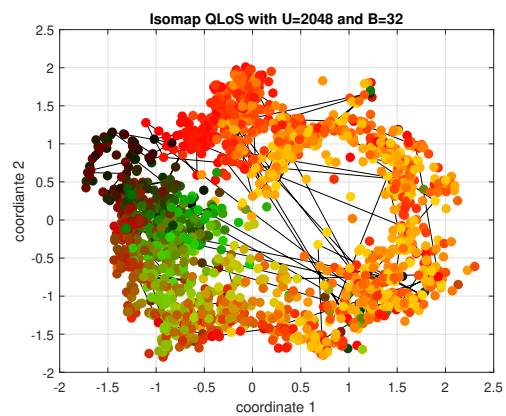


Figure 5.35: The channel chart from Method I with Isomap method under Q-LoS channels.

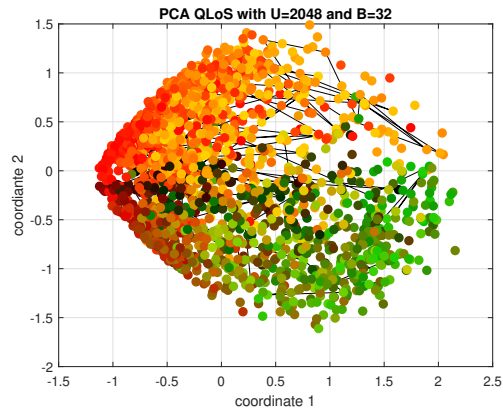


Figure 5.36: The channel chart from Method II with PCA method under Q-LoS channels.

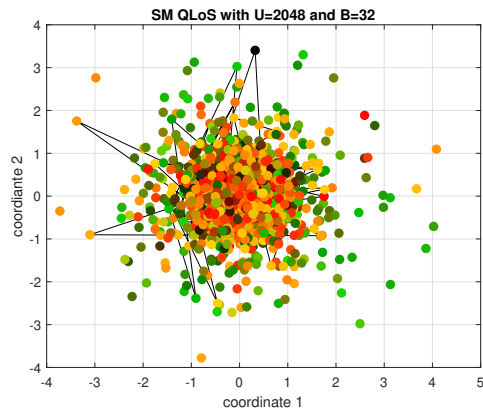


Figure 5.37: The channel chart from Method II with SM method under Q-LoS channels.

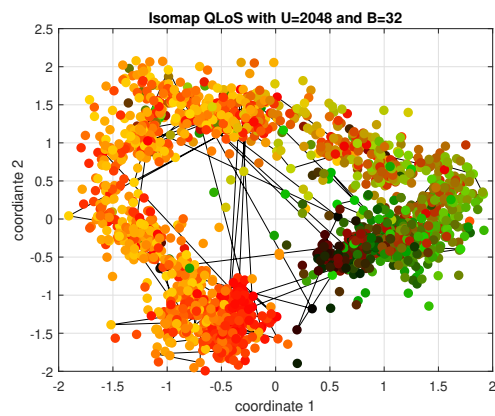


Figure 5.38: The channel chart from Method II with Isomap method under Q-LoS channels.



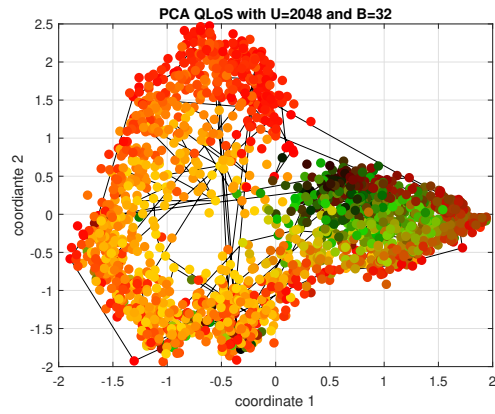


Figure 5.39: The channel chart from Method III with PCA method under Q-LoS channels.

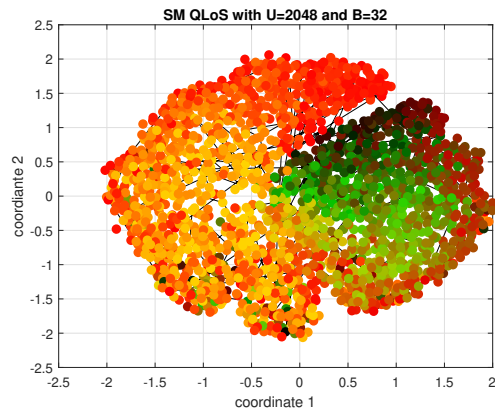


Figure 5.40: The channel chart from Method III with SM method under Q-LoS channels.

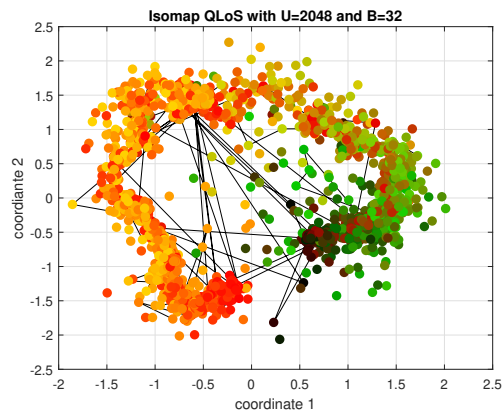


Figure 5.41: The channel chart from Method III with Isomap method under Q-LoS channels.

## 5.2.2 Performance Measures under Q-LoS channels

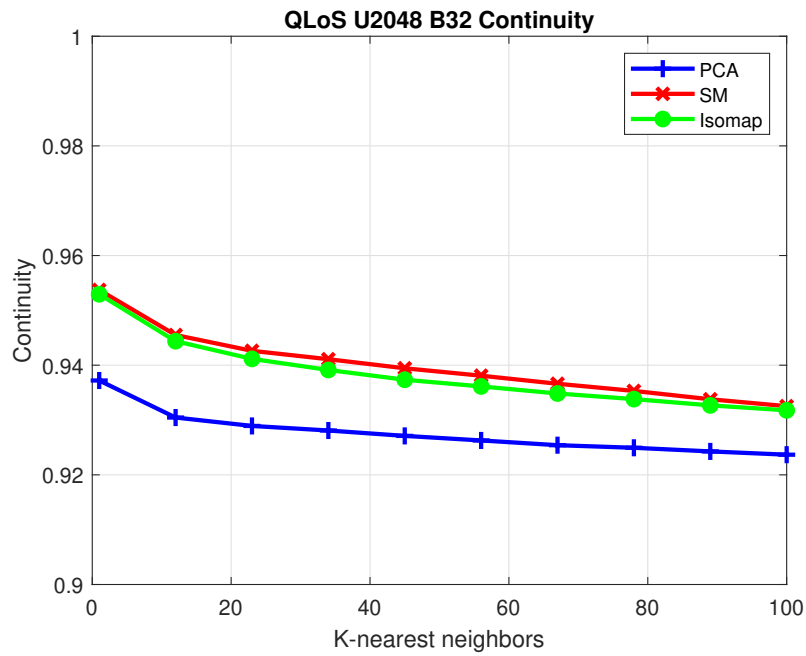


Figure 5.42: The continuity results from Method I with PCA, SM, and Isomap methods under Q-LoS channels.

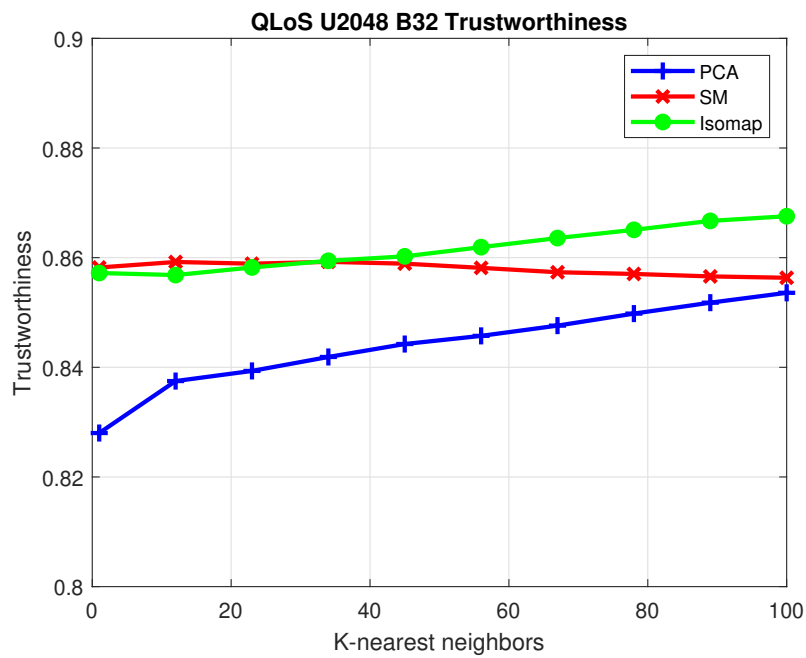


Figure 5.43: The trustworthiness results from Method I with PCA, SM, and Isomap methods under Q-LoS channels.

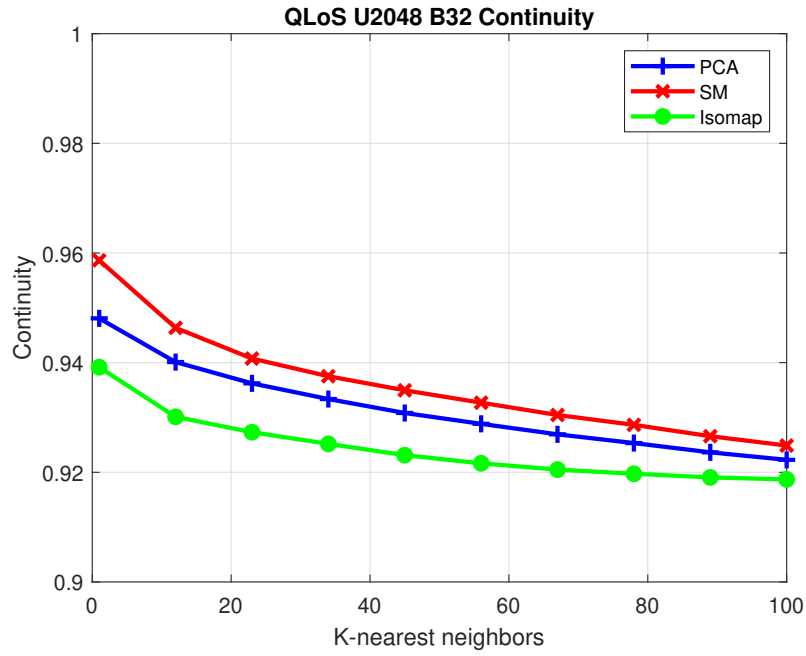


Figure 5.44: The continuity results from Method II with PCA, SM, and Isomap methods under Q-LoS channels.

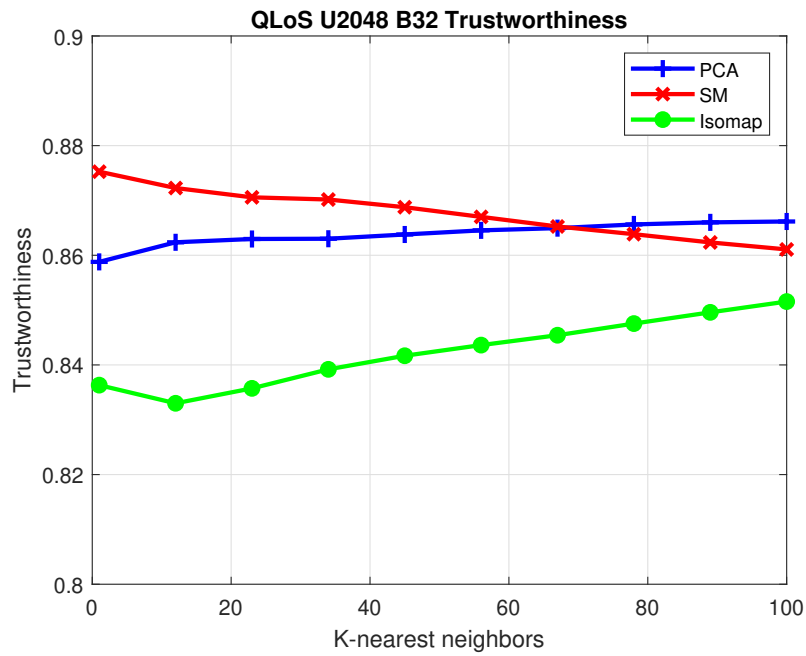


Figure 5.45: The trustworthiness results from Method II with PCA, SM, and Isomap methods under Q-LoS channels.

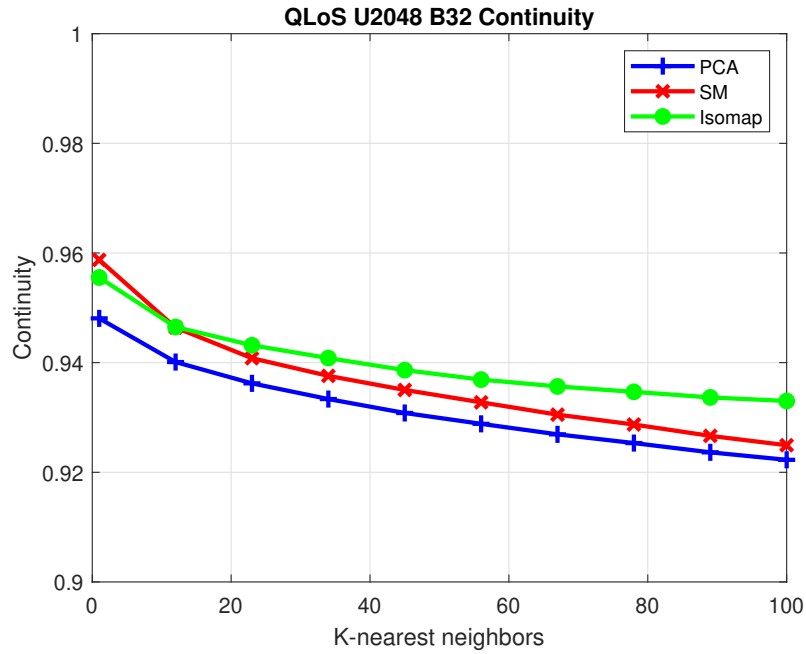


Figure 5.46: The continuity results from Method III with PCA, SM, and Isomap methods under Q-LoS channels.

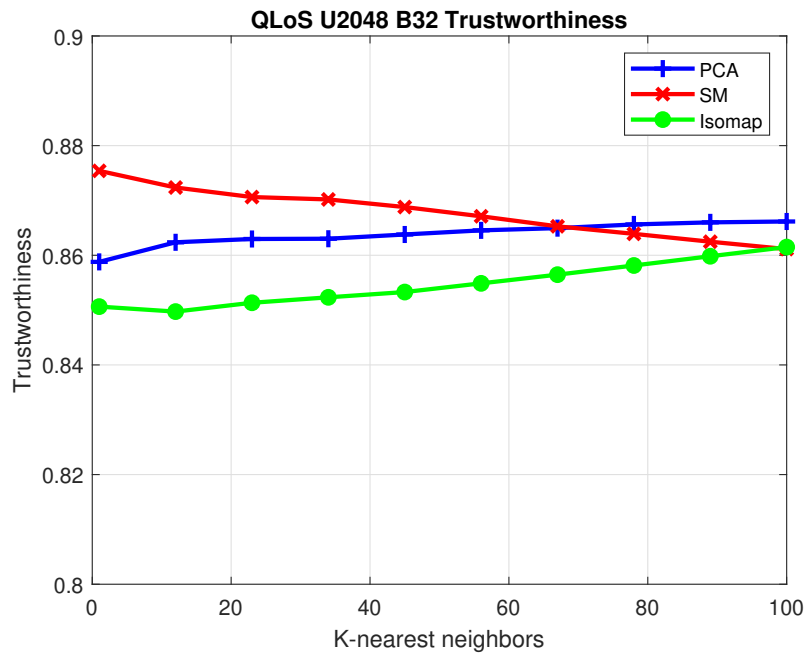


Figure 5.47: The trustworthiness results from Method III with PCA, SM, and Isomap methods under Q-LoS channels.

### 5.2.3 Channel Chart under Q-NLoS channels

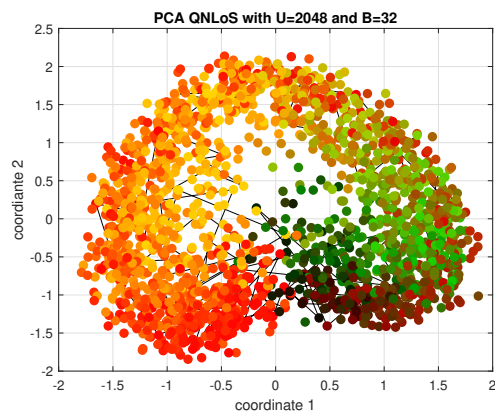


Figure 5.48: The channel chart from Method I with PCA method under Q-NLoS channels.

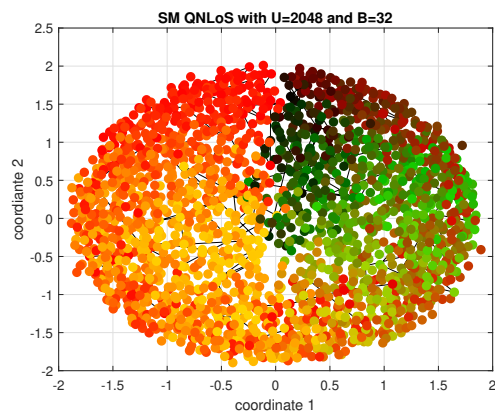


Figure 5.49: The channel chart from Method I with SM method under Q-NLoS channels.

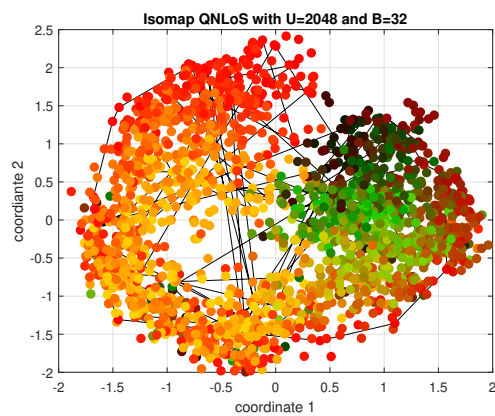


Figure 5.50: The channel chart from Method I with Isomap method under Q-NLoS channels.

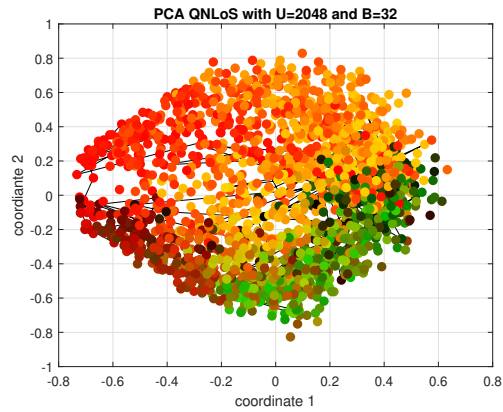


Figure 5.51: The channel chart from Method II with PCA method under Q-NLoS channels.

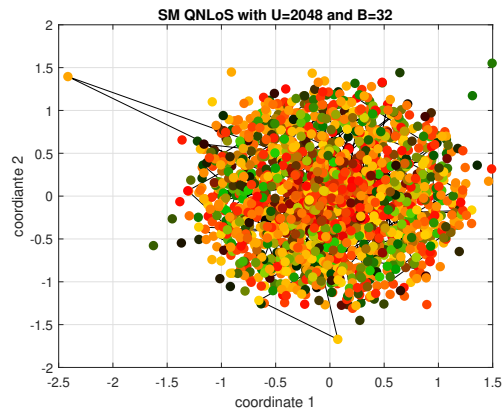


Figure 5.52: The channel chart from Method II with SM method under Q-NLoS channels.

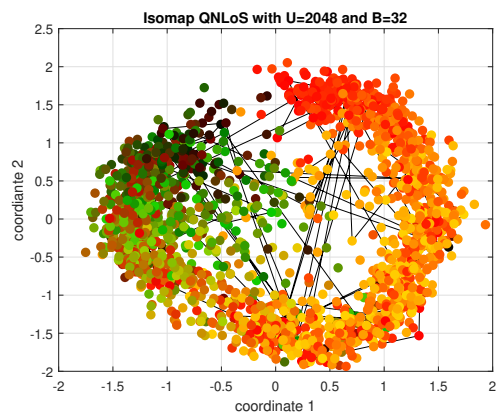


Figure 5.53: The channel chart from Method II with Isomap method under Q-NLoS channels.

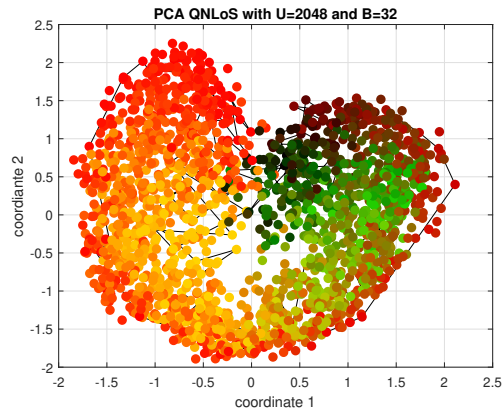


Figure 5.54: The channel chart from Method III with PCA method under Q-NLoS channels.

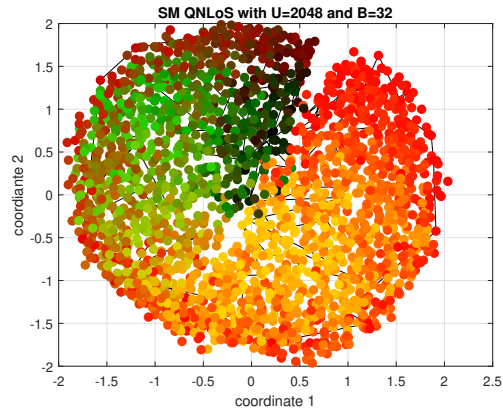


Figure 5.55: The channel chart from Method III with SM method under Q-NLoS channels.

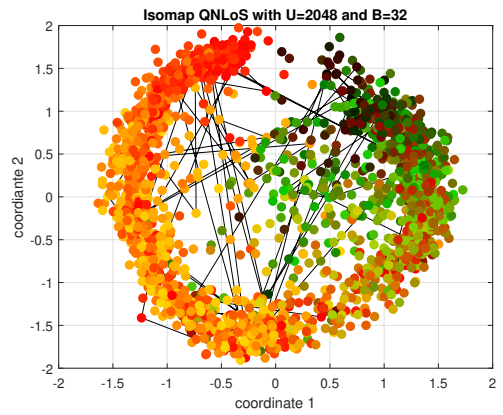


Figure 5.56: The channel chart from Method III with Isomap method under Q-NLoS channels.

## 5.2.4 Performance Measures under Q-NLoS channels

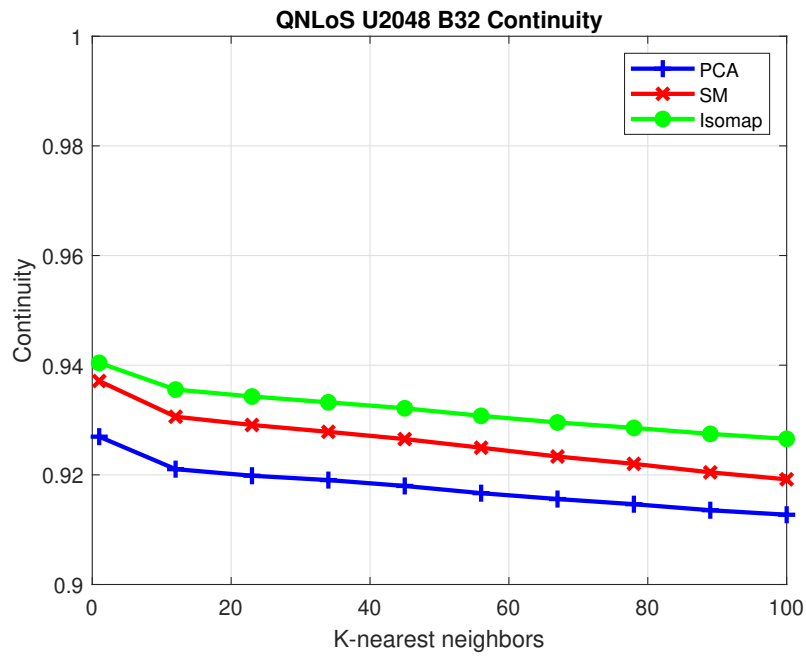


Figure 5.57: The continuity results from Method I with PCA, SM, and Isomap methods under Q-NLoS channels.

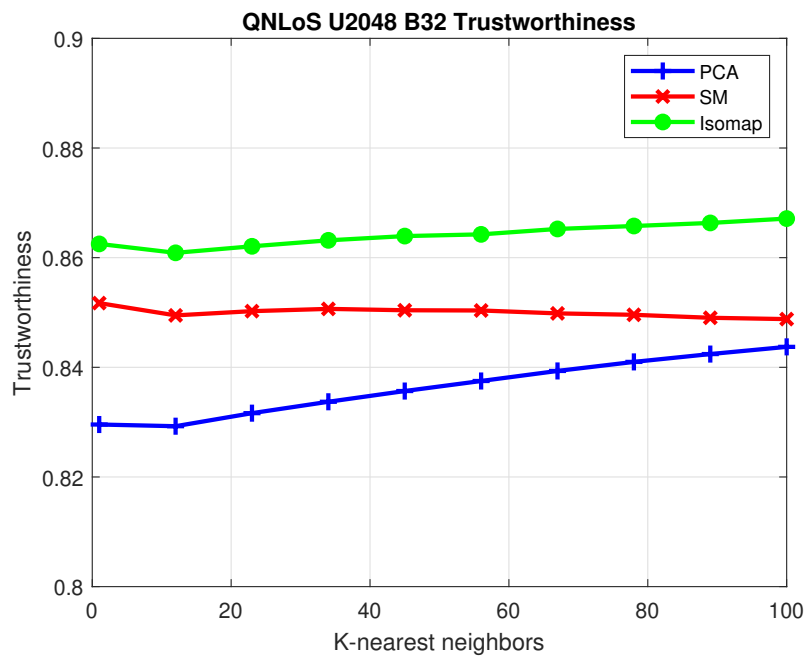


Figure 5.58: The trustworthiness results from Method I with PCA, SM, and Isomap methods under Q-NLoS channels.



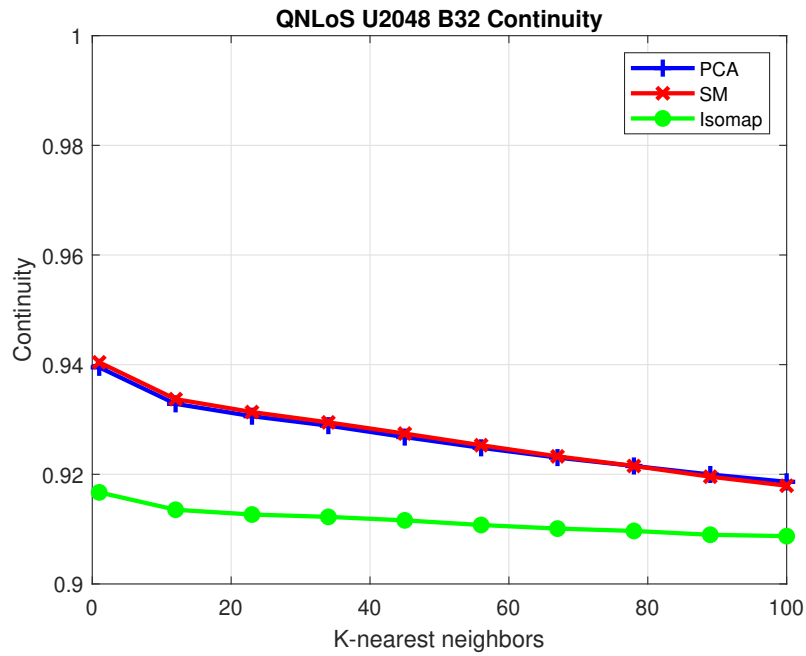


Figure 5.59: The continuity results from Method II with PCA, SM, and Isomap methods under Q-NLoS channels.

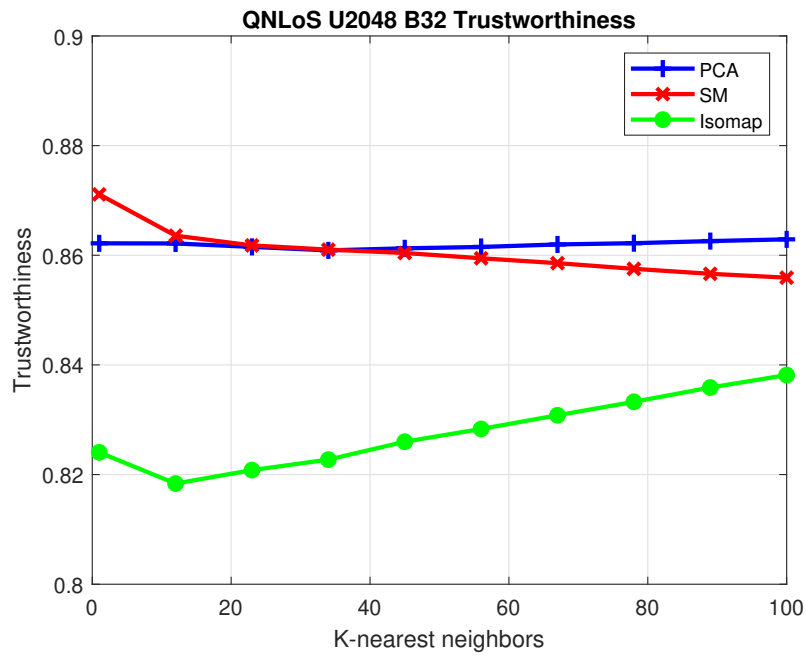


Figure 5.60: The trustworthiness results from Method II with PCA, SM, and Isomap methods under Q-NLoS channels.

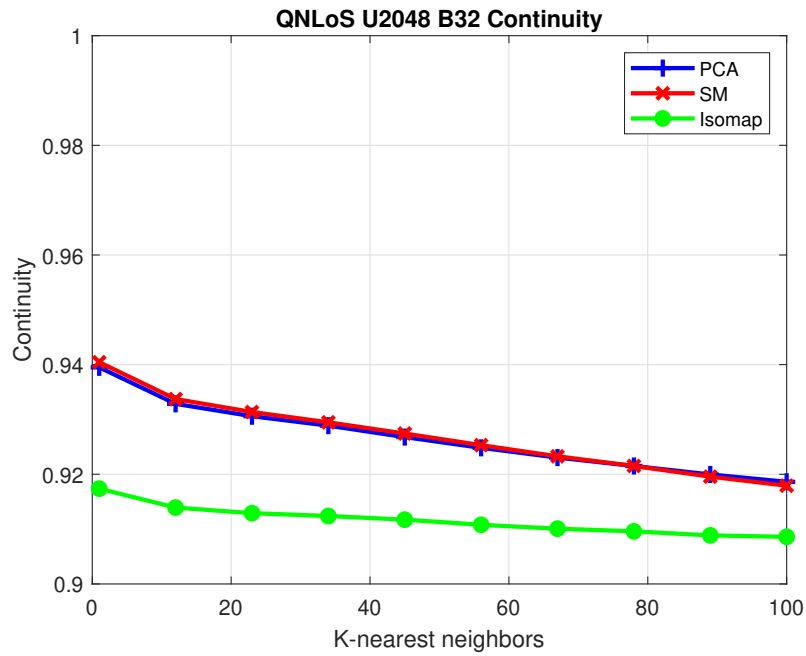


Figure 5.61: The continuity results from Method III with PCA, SM, and Isomap methods under Q-NLoS channels.

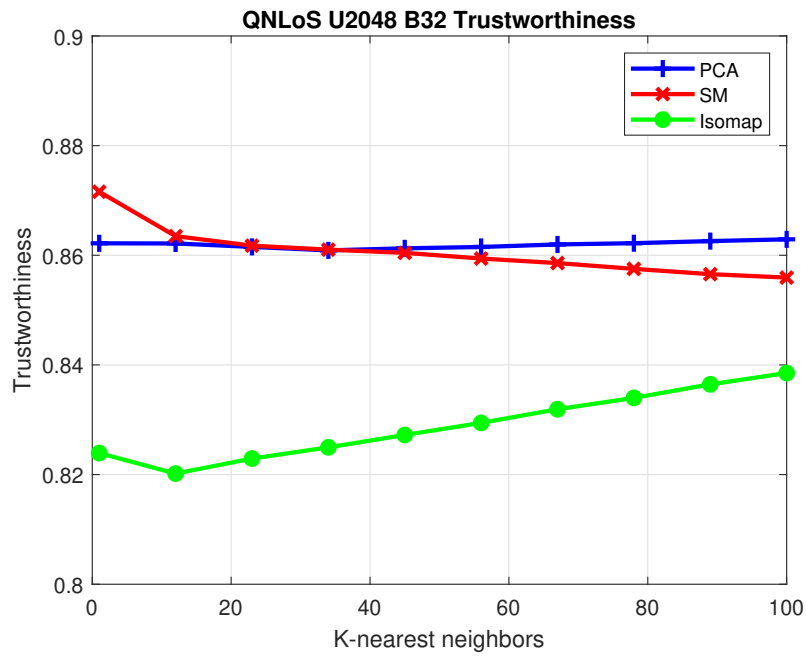


Figure 5.62: The trustworthiness results from Method III with PCA, SM, and Isomap methods under Q-NLoS channels.

### 5.3 Results of Simulation III

First, we consider the results under the Q-LoS channels. Fig. 5.64 - Fig. 5.66 are the channel charts with Method I of PCA method, SM method, and Isomap method. The channel chart from the SM method is the best among these three channel charts. In Fig. 5.73, the CT results from the PCA method and the SM method are close. When the number of the nearest neighbor is small,  $K \leq 67$ , the CT results from the Isomap method are the best, while when the number of the nearest neighbor increases,  $K > 67$ , the CT results from the Isomap method are the worst. In Fig. 5.73, the TW results from the Isomap method are the best, while the TW results from the PCA method are the worst. Fig. 5.67 - Fig. 5.69 are the channel charts with Method II of PCA method, SM method, and Isomap method. The channel charts from Method II with the PCA method and the SM method are worse than those from Method I with the PCA method and the SM method, respectively, while the channel chart from Method II with the Isomap method is similar to this from Method I with the Isomap method. In Fig. 5.75, the CT results from Method II with the Isomap are close to those from Method I with the Isomap method, while the CT results from Method II with the PCA method and the SM method are much lower than those from Method I with the PCA method and the SM method. In Fig. 5.76, all the TW results from Method II are lower than those corresponding results from Method I. When the number of the nearest neighbors is less than 35, the TW results from the SM method are the highest, while the number of the nearest neighbors is greater than 35, the TW results from the Isomap method are the highest among all three dimensionality reduction methods. Fig. 5.70 - Fig. 5.72 are the channel charts with Method III of PCA method, SM method, and Isomap method. The channel charts from Method III are similar to those corresponding channel charts from Method II, but seem even worse. In Fig. 5.77, the CT results from the Isomap method are the best. The CT results from Method III with the Isomap method and the SM method are close to those from Method II with the Isomap method and the SM method, respectively,

while the CT results from Method III with the PCA method are much worse than those from Method II with the PCA method. In Fig. 5.78, the TW results from Method III with the PCA method are much better than those from Method II with the PCA method, the TW results from Method III with the Isomap methods are close to those from Method II with the Isomap method, and the TW results from Method III with the SM method are much worse than those from Method II with the SM method.

And second, we consider the results under the Q-NLoS channels. Fig. 5.79 - Fig. 5.81 are the channel charts with Method I of PCA method, SM method, and Isomap method. The channel chart from the PCA method and the Isomap method looks close to the channel chart from the SM method. But the channel chart from the SM method still looks the best. However, in Fig. 5.88 and Fig. 5.89, the CT and TW results from the Isomap method are the best among three dimensionality reduction methods. The CT and TW results from the PCA method and the SM method are close. Fig. 5.82 - Fig. 5.84 are the channel charts with Method II of PCA method, SM method, and Isomap method. The points in the channel charts from Method II are more scattered than those in the corresponding channel charts from Method I. In Fig. 5.90 and Fig. 5.91, the CT and TW results from the PCA method are the best, and are close to those from Method I with the PCA method, and the CT and TW results from the SM method and the Isomap method are close. Fig. 5.85 - Fig. 5.87 are the channel charts with Method III of PCA method, SM method, and Isomap method. The channel charts from Method III look similar to those from Method II, but the points are more scattered. In Fig. 5.92 and Fig. 5.93, the CT and TW results from the PCA method are the best among those corresponding results. And in Fig. 5.92, when the number of the nearest neighbors is less than 78, the CT results from the SM method are better than those from the Isomap method, while when the number of the nearest neighbors is greater than 78, the CT results from the Isomap method are better than those from the SM method. In Fig. 5.93, when the number of the nearest neighbors is less than 67, the TW results from the SM method are better than those from the Isomap method, while when the number of

the nearest neighbors is greater than 67, the TW results from the Isomap method are better than those from the SM method.

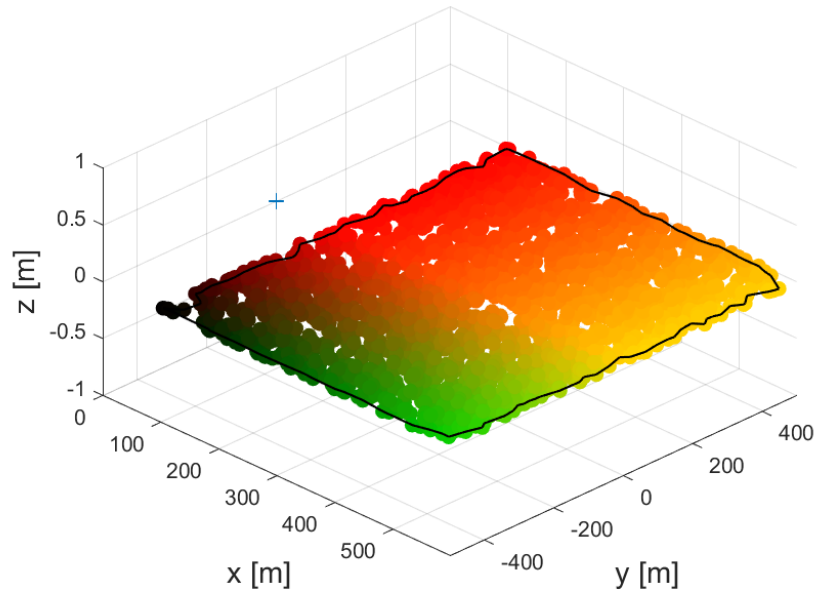


Figure 5.63: The user equipments' location in the real space in Simulation III. The colored points represent the user equipments, and the cross point represents the ULA.

Under Q-LoS channels, the CT results with Method I among three dimensionality reduction methods are close, while the TW results with Isomap and SM using Method I are much better than these with PCA. The CT and TW results with Isomap using Method II are slightly better than those from PCA and SM. The results with Isomap and PCA using Method III are better than those from SM. It seems that the Isomap method shows advantages in improving the performance of the CT and TW in multisubcarrier cases under Q-LoS channels. However, we cannot observe these phenomena under Q-NLoS channels. Under Q-NLoS channels, the CT and TW results with the Isomap using Method I are better than the corresponding results from the other two dimensionality reduction methods while the CT and TW results with PCA using Method II and Method III are much better than the corresponding results from the other two dimensionality reduction methods. Although it seems that the KS results of Simulation III follow the same rules that we concluded in Section 5.1 and Section 5.2,

unlike the KS results from Simulation I and Simulation II, the KS results of Simulation III get much worse, increasing by 20% in general.

	Method	I	II	III
Q-LoS	PCA	0.4916	0.6069	0.5847
	SM	0.5075	0.5065	0.5211
	Isomap	0.5417	0.4936	0.4876
Q-NLoS	PCA	0.5222	0.5558	0.5515
	SM	0.5056	0.4857	0.4911
	Isomap	0.5431	0.4790	0.4779

Table 5.3: The performances of KS under the Q-LoS channels and the Q-NLoS channels. Method I represents the CSI extracted features method proposed in [7]. Method II represents the distance measurement method proposed in [5]. Method III represents the correlation matrix distance method.

### 5.3.1 Channel Chart under Q-LoS

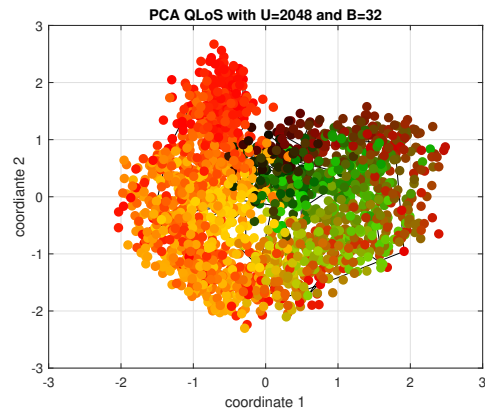


Figure 5.64: The channel chart from Method I with PCA method under Q-LoS channels.

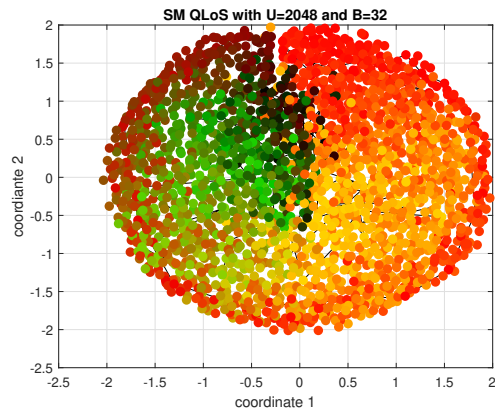


Figure 5.65: The channel chart from Method I with SM method under Q-LoS channels.

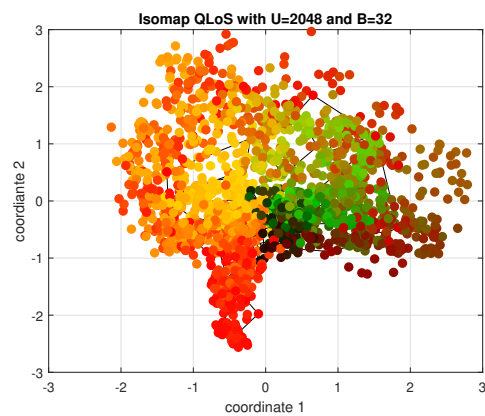


Figure 5.66: The channel chart from Method I with Isomap method under Q-LoS channels.

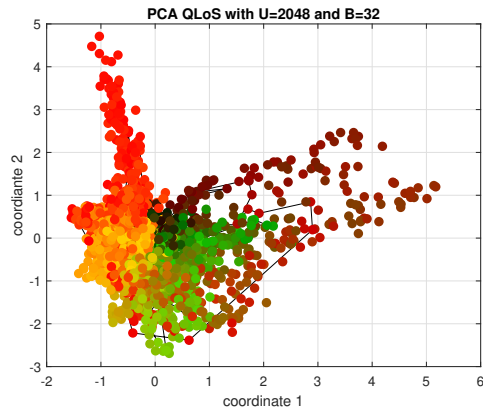


Figure 5.67: The channel chart from Method II with PCA method under Q-LoS channels.

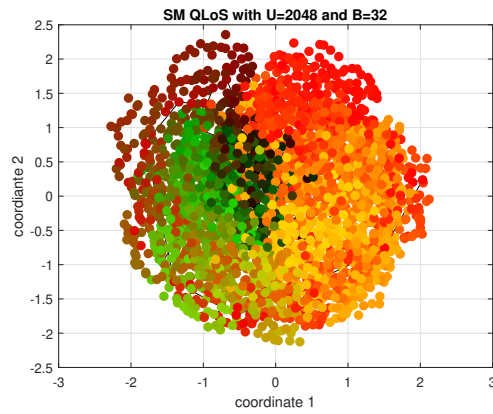


Figure 5.68: The channel chart from Method II with SM method under Q-LoS channels.

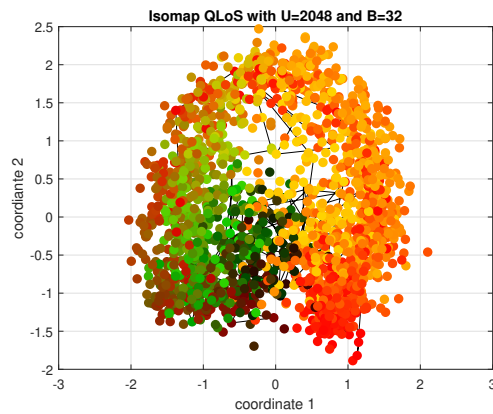


Figure 5.69: The channel chart from Method II with Isomap method under Q-LoS channels.



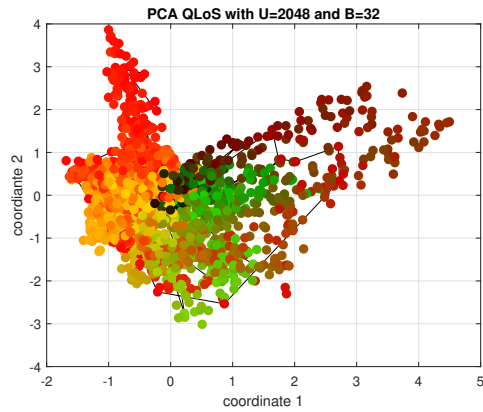


Figure 5.70: The channel chart from Method III with PCA method under Q-LoS channels.

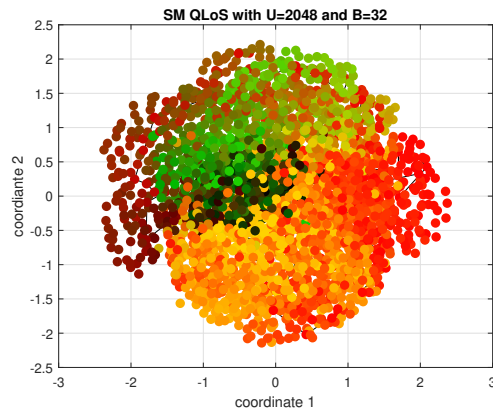


Figure 5.71: The channel chart from Method III with SM method under Q-LoS channels.

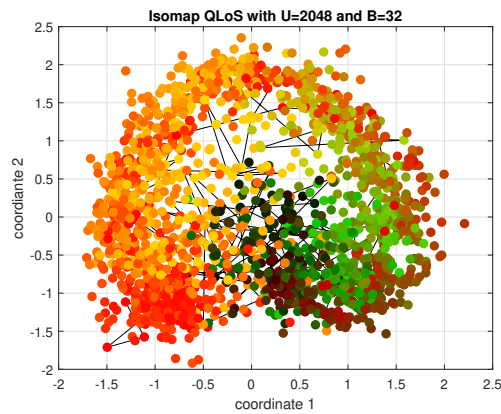


Figure 5.72: The channel chart from Method III with Isomap method under Q-LoS channels.

### 5.3.2 Performance Measures under Q-LoS channels

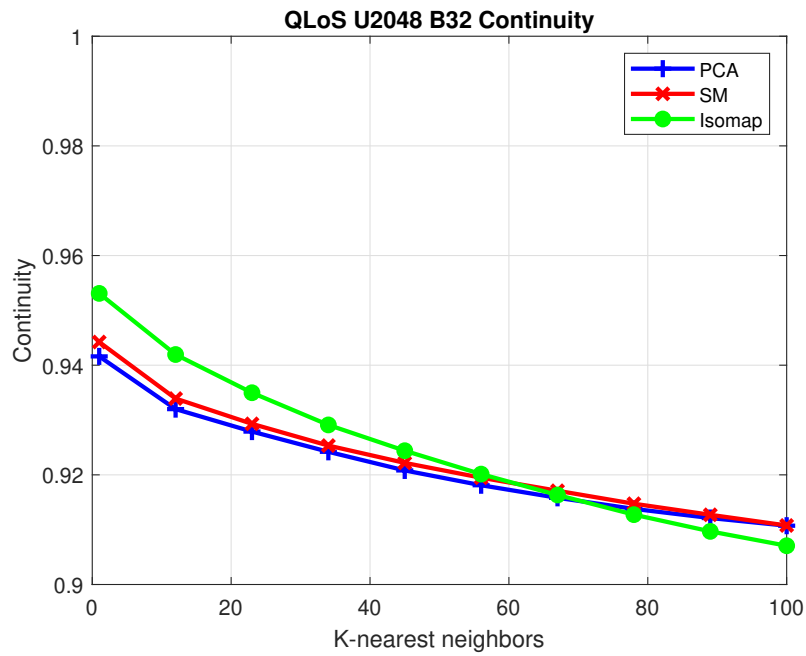


Figure 5.73: The continuity results from Method I with PCA, SM, and Isomap methods under Q-LoS channels.

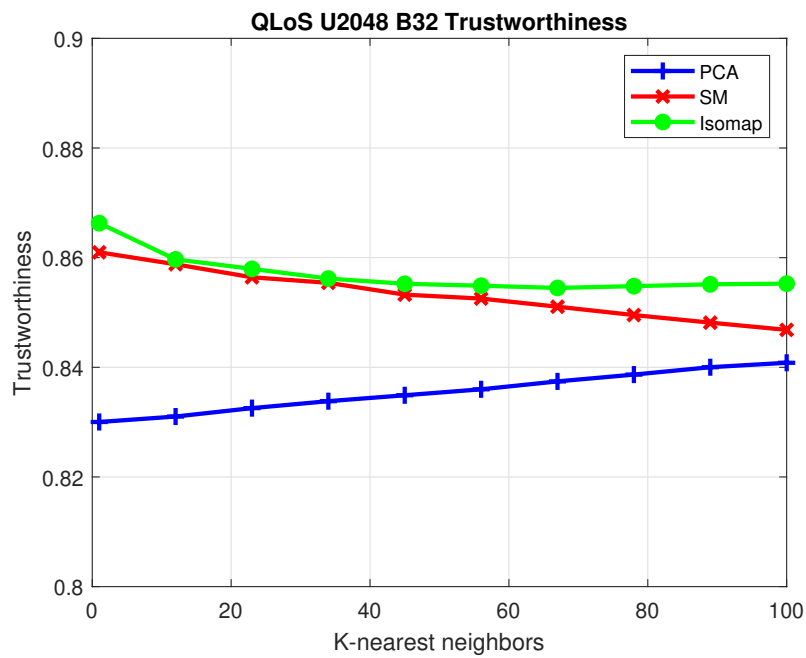


Figure 5.74: The trustworthiness results from Method I with PCA, SM, and Isomap methods under Q-LoS channels.

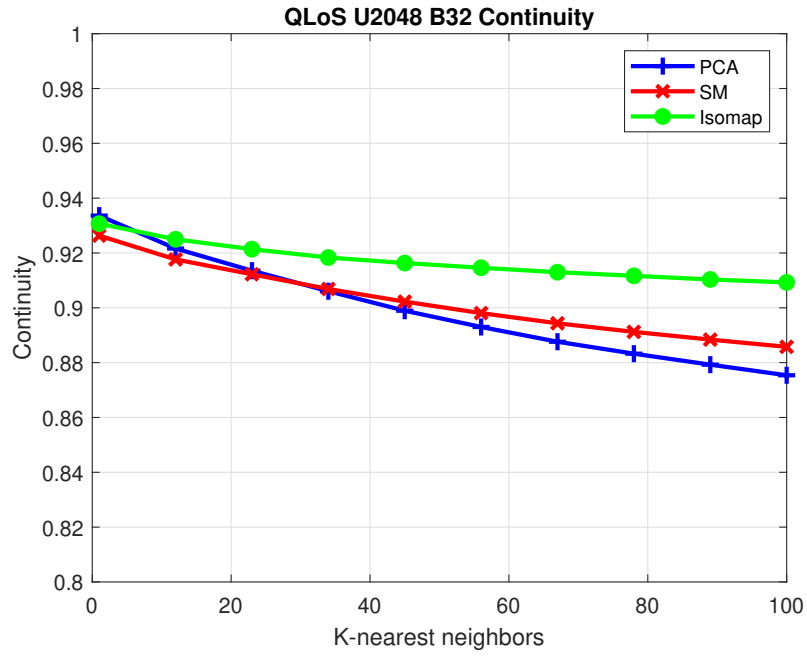


Figure 5.75: The continuity results from Method II with PCA, SM, and Isomap methods under Q-LoS channels.

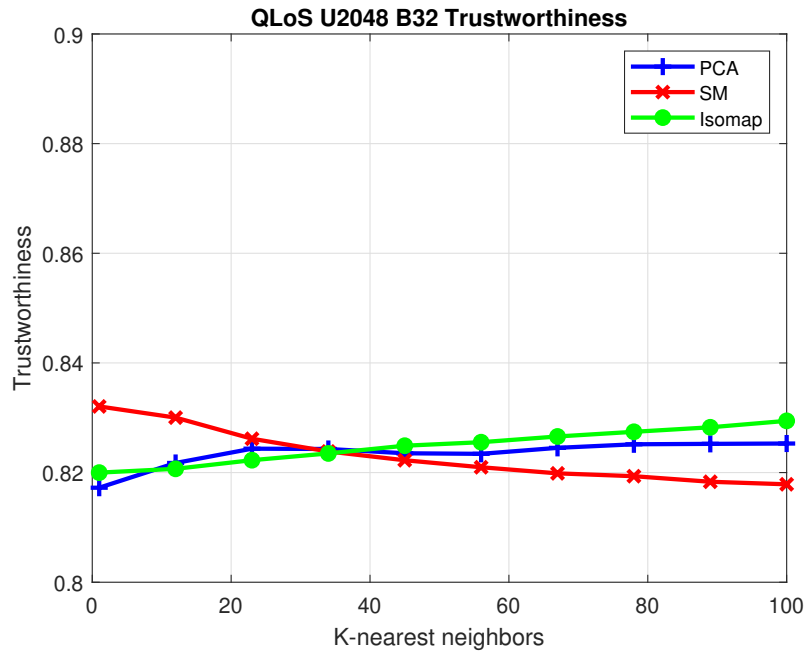


Figure 5.76: The trustworthiness results from Method II with PCA, SM, and Isomap methods under Q-LoS channels.

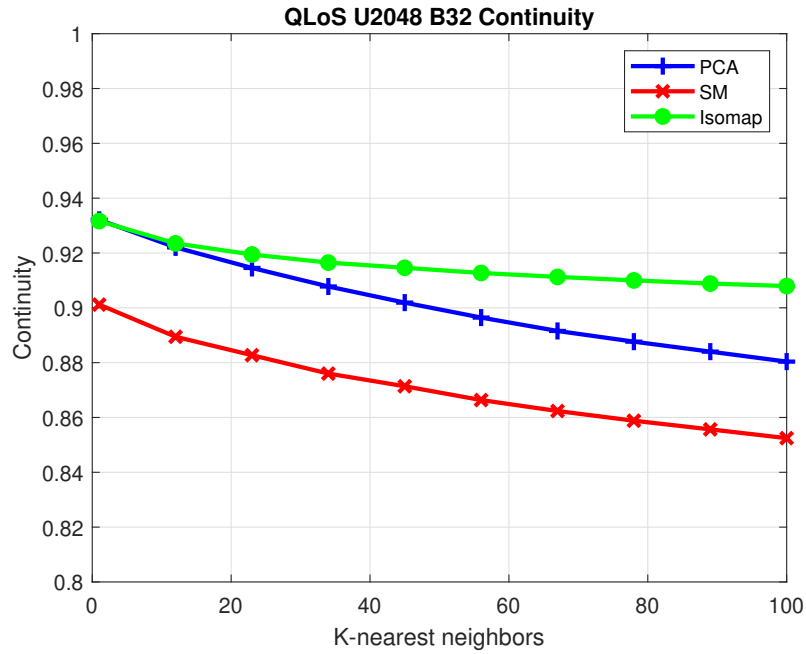


Figure 5.77: The continuity results from Method III with PCA, SM, and Isomap methods under Q-LoS channels.

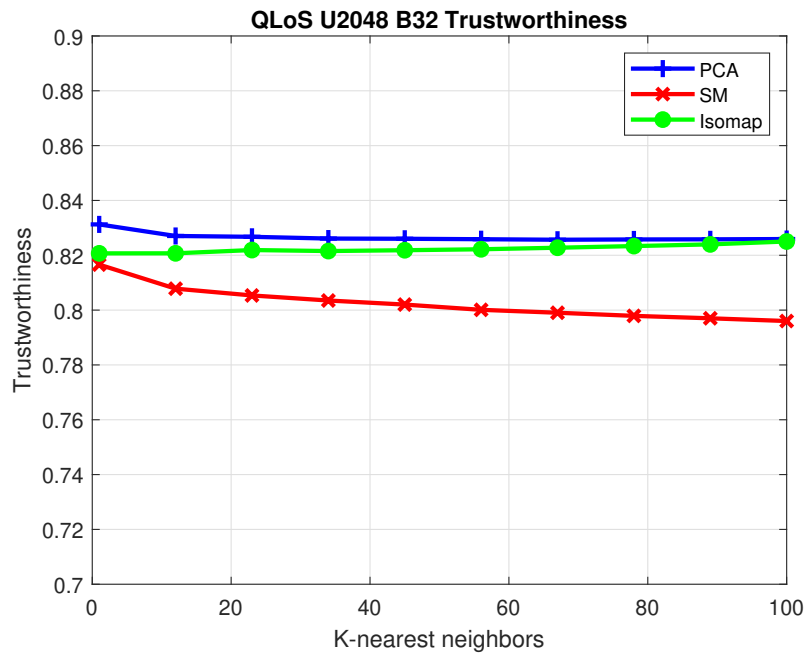


Figure 5.78: The trustworthiness results from Method III with PCA, SM, and Isomap methods under Q-LoS channels.

### 5.3.3 Channel Chart under Q-NLoS channels

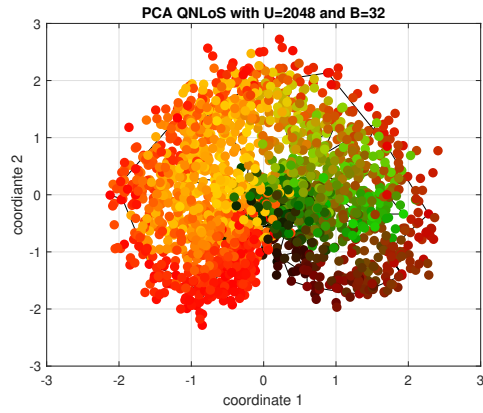


Figure 5.79: The channel chart from Method I with PCA method under Q-NLoS channels.

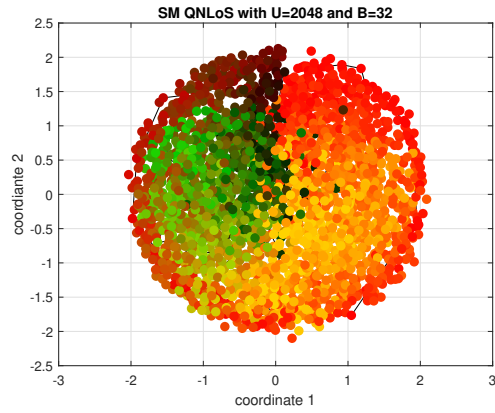


Figure 5.80: The channel chart from Method I with SM method under Q-NLoS channels.

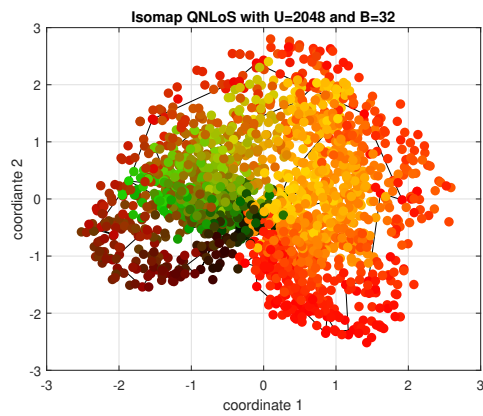


Figure 5.81: The channel chart from Method I with Isomap method under Q-NLoS channels.

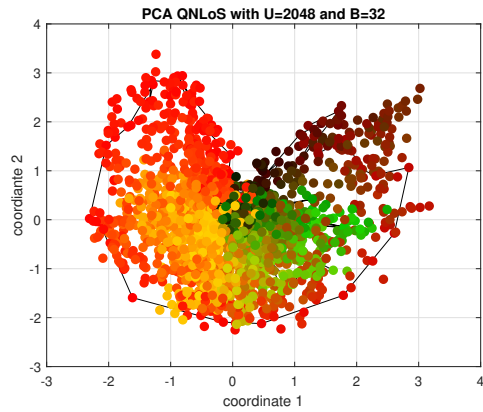


Figure 5.82: The channel chart from Method II with PCA method under Q-NLoS channels.

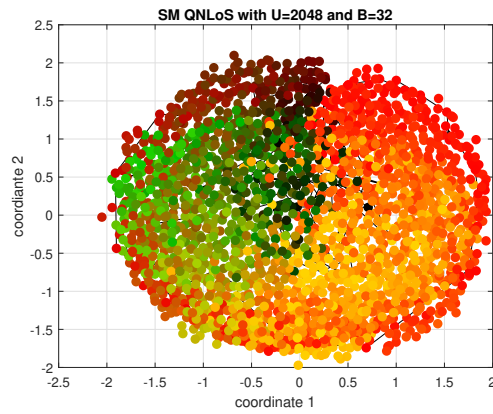


Figure 5.83: The channel chart from Method II with SM method under Q-NLoS channels.

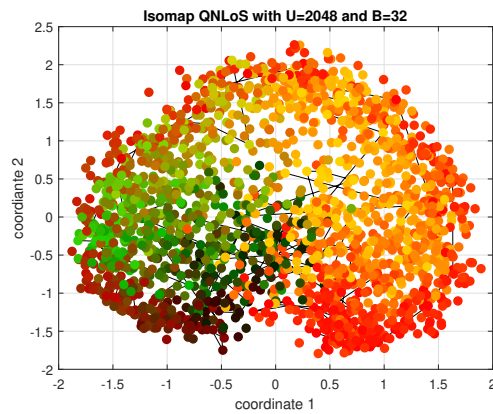


Figure 5.84: The channel chart from Method II with Isomap method under Q-NLoS channels.

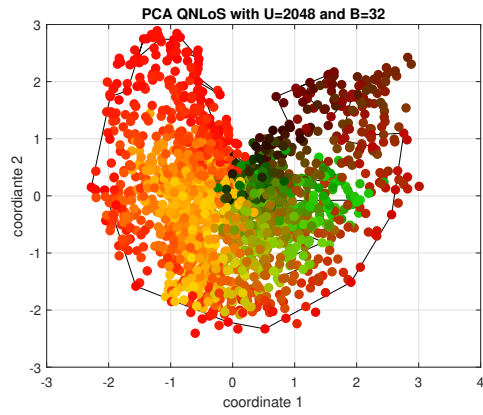


Figure 5.85: The channel chart from Method III with PCA method under Q-NLoS channels.

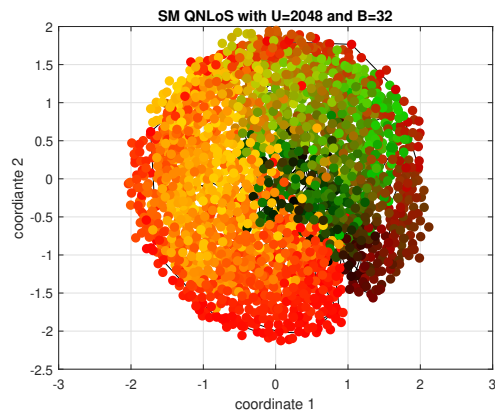


Figure 5.86: The channel chart from Method III with SM method under Q-NLoS channels.

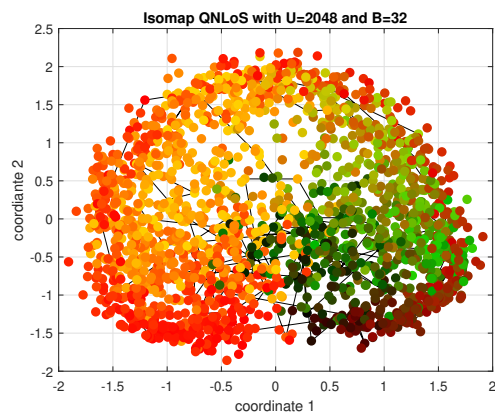


Figure 5.87: The channel chart from Method III with Isomap method under Q-NLoS channels.

### 5.3.4 Performance Measures under Q-NLoS channels

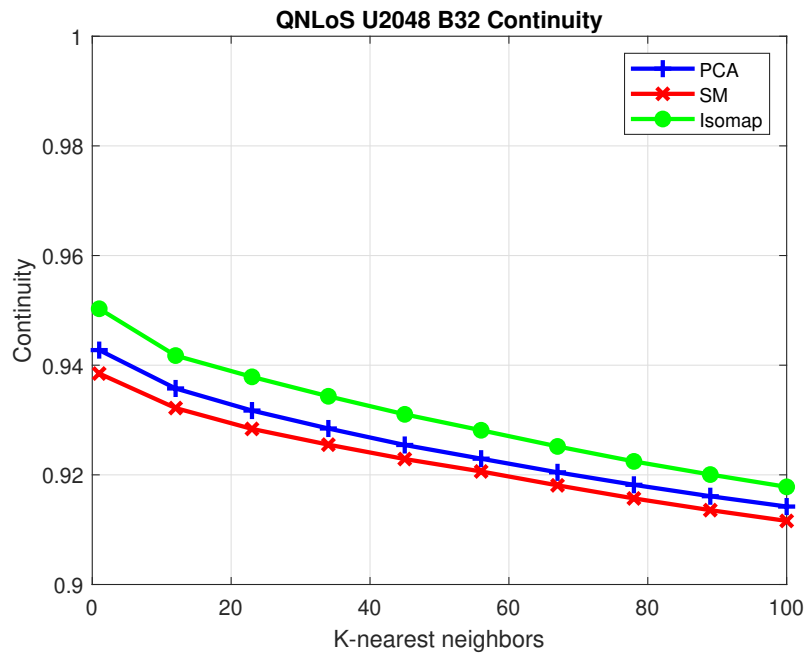


Figure 5.88: The continuity results from Method I with PCA, SM, and Isomap methods under Q-NLoS channels.

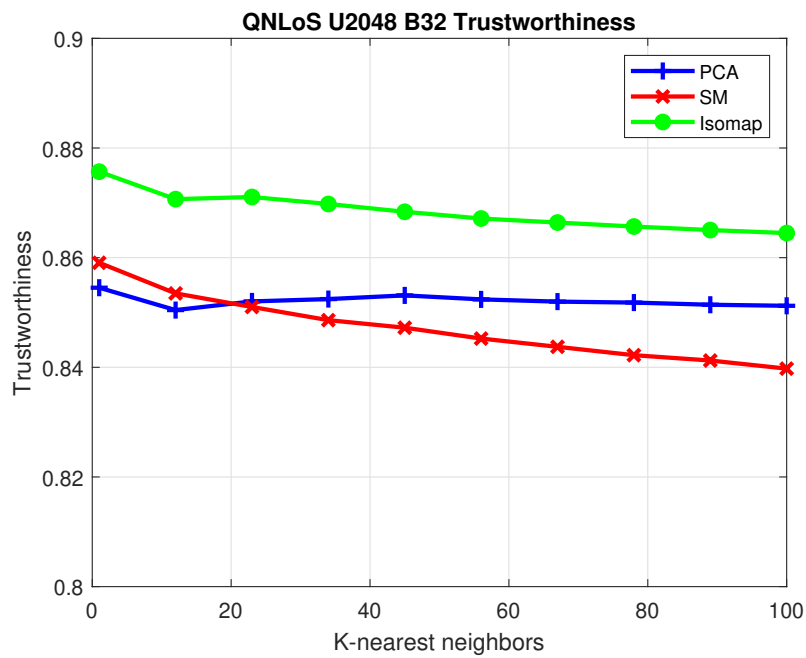


Figure 5.89: The trustworthiness results from Method I with PCA, SM, and Isomap methods under Q-NLoS channels.



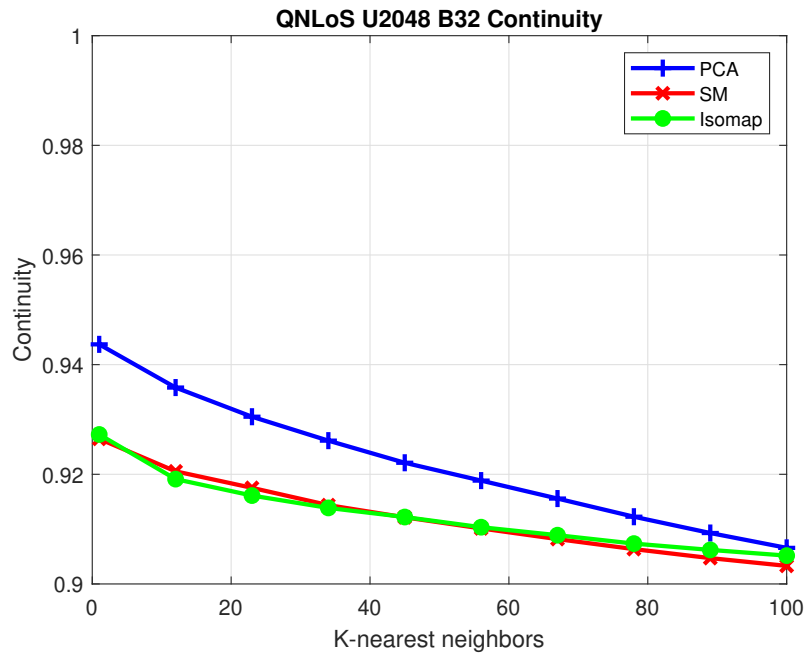


Figure 5.90: The continuity results from Method II with PCA, SM, and Isomap methods under Q-NLoS channels.

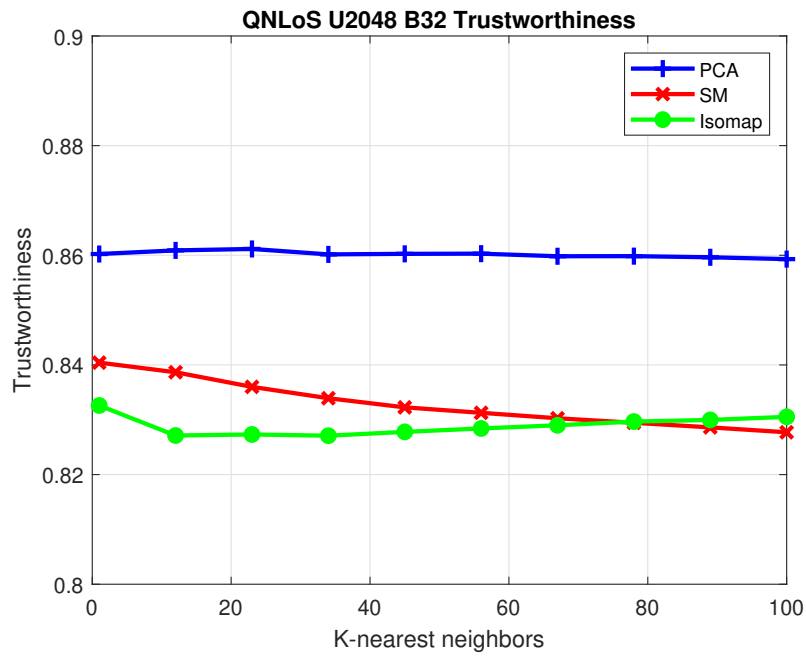


Figure 5.91: The trustworthiness results from Method II with PCA, SM, and Isomap methods under Q-NLoS channels.

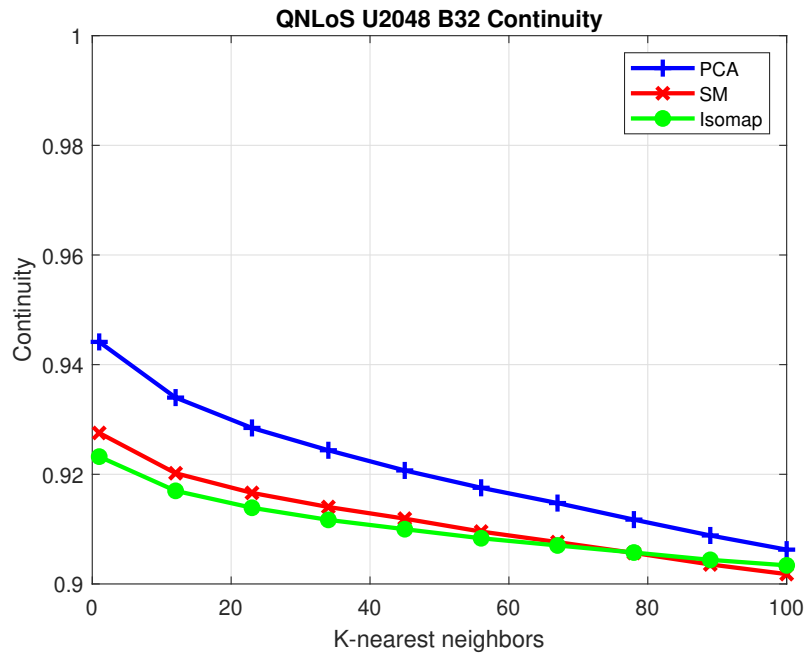


Figure 5.92: The continuity results from Method III with PCA, SM, and Isomap methods under Q-NLoS channels.

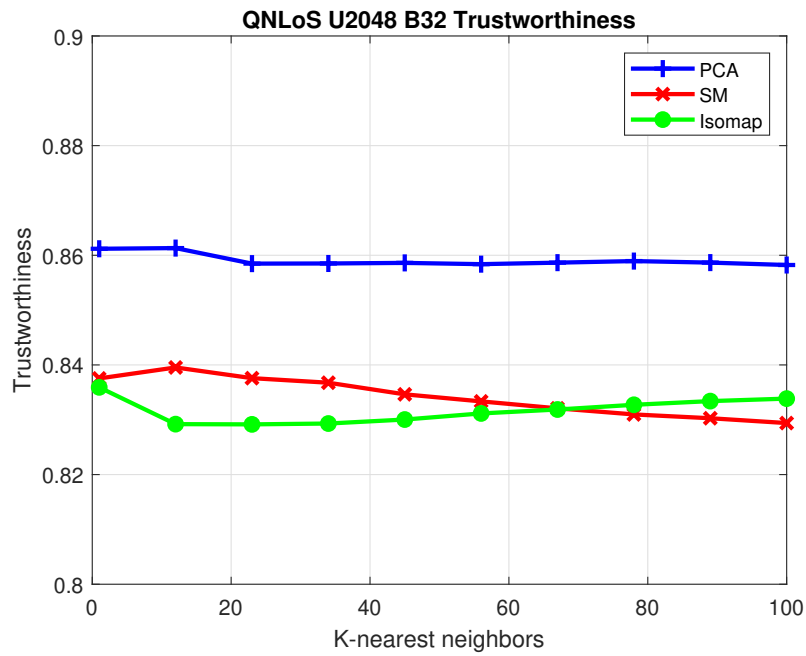


Figure 5.93: The trustworthiness results from Method III with PCA, SM, and Isomap methods under Q-NLoS channels.

Based on all the results above, we find that most of the CT results are in the range between 0.9 and 1, most of the TW results are in the range between 0.8 and 0.9, and the most of the KS results are in the range between 0.4 and 0.6. We could give some general conclusions here. First, we find that, the CT and TW results with Isomap using Method I, the CSI feature extraction method, are better than those corresponding results with PCA and SM using Method I. Second, the CT and TW results with PCA and SM with Method II, the efficient distance measure method, and Method III, the correlation matrix distance method, are much better than those with Isomap. And third, Method I, CSI feature extraction method, combining with the Isomap method, could provide better CT and TW results while Method II, the efficient distance measure method, or Method III, the correlation matrix distance method, combining with the PCA method or the SM method, could give relative stable and better performance in both CT and TW results. In our simulations, CT and TW results from these two are close. However, Method I together with the Isomap method might have shortcomings in time cost and memory cost. The complexity of the Method I is at least  $O(M^2N^2)$  while the complexity of the Method II or the Method III is  $O(MN^2)$ . The computation of the Method I is growing squarely compared with the Method II or the Method III, when  $M$ , the product of the number of antennas and the number of the subcarriers, increases. As for the KS results, only the Isomap method with the Method II and Method III, show better performance than other alternatives.

# Chapter 6

## Conclusion

In this thesis, we discussed three CSI pre-processing methods, the CSI feature extraction method, the efficient distance measure method, and the correlation matrix distance method, together with three common-used dimensionality reduction methods, PCA, SM, and Isomap. We simulated the nine alternatives under two channel models, line-of-sight and non-line-of-sight Quadriga channels, to find out the best method for generating the channel chart. In order to quantify the performance of the channel chart more clearly, we discussed three performance measures to analyze the performance of the channel chart generated from each combinations. Generally, we could conclude that the Method II, efficient distance method, combining with the PCA or SM methods, could stably show the better continuity and trustworthiness performance with less computation complexity while the Method III, correlation matrix distance method together with the Isomap method could show the best Kruskal's stress performance.

# Bibliography

- [1] F. Burkhardt, S. Jaeckel, E. Eberlein, and R. Prieto-Cerdeira. QuaDRiGa: A MIMO channel model for land mobile satellite. In *The 8th European Conference on Antennas and Propagation (EuCAP 2014)*, pages 1274–1278, 2014.
- [2] P. Ferrand, A. Decurninge, L. G. Ordoñez, and M. Guillaud. Triplet-based wireless channel charting. In *GLOBECOM 2020-2020 IEEE Global Communications Conference*, pages 1–6. IEEE, 2020.
- [3] M. Herdin and E. Bonek. *A MIMO correlation matrix based metric for characterizing non-stationarity*. na, 2004.
- [4] J. B. Kruskal. Multidimensional scaling by optimizing goodness of fit to a nonmetric hypothesis. *Psychometrika*, 29(1):1–27, 1964.
- [5] L. Le Magoarou. Efficient channel charting via phase-insensitive distance computation. *IEEE Wireless Communications Letters*, 10(12):2634–2638, 2021.
- [6] F. Pedregosa, G. Varoquaux, A. Gramfort, V. Michel, B. Thirion, O. Grisel, M. Blondel, P. Prettenhofer, R. Weiss, V. Dubourg, J. Vanderplas, A. Passos, D. Cournapeau, M. Brucher, M. Perrot, and Édouard Duchesnay. Scikit-learn: Machine learning in python. *Journal of Machine Learning Research*, 12(85):2825–2830, 2011.
- [7] C. Studer, S. Medjkouh, E. Gonultas, T. Goldstein, and O. Tirkkonen. Channel charting: Locating users within the radio environment using channel state information. *IEEE Access*, 6:47682–47698, 2018.
- [8] J. B. Tenenbaum, V. De Silva, and J. C. Langford. A global geometric framework for nonlinear dimensionality reduction. *Science*, 290(5500):2319–2323, 2000.